

See discussions, stats, and author profiles for this publication at: <https://www.researchgate.net/publication/26852410>

Structural and Electronic Properties of Reduced Transition Metal Oxide Clusters, M₃O₈ and M₃O₈₋ (M = Cr, W), from Photoelectron Spectroscopy and Quantum Chemical Calculations

ARTICLE *in* THE JOURNAL OF PHYSICAL CHEMISTRY A · SEPTEMBER 2009

Impact Factor: 2.69 · DOI: 10.1021/jp9082008 · Source: PubMed

CITATIONS

42

READS

25

4 AUTHORS, INCLUDING:



Lai-Sheng Wang

Brown University

434 PUBLICATIONS 18,855 CITATIONS

[SEE PROFILE](#)



David A Dixon

University of Alabama

766 PUBLICATIONS 22,202 CITATIONS

[SEE PROFILE](#)

Structural and Electronic Properties of Reduced Transition Metal Oxide Clusters, M_3O_8 and $M_3O_8^-$ ($M = Cr, W$), from Photoelectron Spectroscopy and Quantum Chemical Calculations

Shenggang Li,[†] Hua-Jin Zhai,[‡] Lai-Sheng Wang,^{*‡} and David A. Dixon^{*†}

Chemistry Department, The University of Alabama, Shelby Hall, Box 870336, Tuscaloosa, Alabama 35487-0336, Department of Physics, Washington State University, 2710 University Drive, Richland, Washington 99354, and Chemical & Materials Sciences Division, Pacific Northwest National Laboratory, MS K8-88, P.O. Box 999, Richland, Washington 99352

Received: August 25, 2009

We report a comparative study of reduced transition metal oxide clusters, $M_3O_8^-$ ($M = Cr, W$) anions and their neutrals, via anion photoelectron spectroscopy (PES) and density functional theory (DFT) and molecular orbital theory (CCSD(T)) calculations. Well-resolved PES spectra are obtained for $M_3O_8^-$ ($M = Cr, W$) at 193 and 157 nm photon energies. Different PES spectra are observed for $M = Cr$ versus $M = W$. Extensive DFT and CCSD(T) calculations are performed to locate the ground and low-lying excited states for the neutrals and anions. The ground states of Cr_3O_8 and $Cr_3O_8^-$ are predicted to be the 3B_2 and 4B_2 states of a C_{2v} structure, respectively, revealing ferromagnetic spin coupling for Cr 3d electrons. In contrast, the ground states of W_3O_8 and $W_3O_8^-$ are predicted to be the $^1A'$ state (C_s symmetry) and the 2A_1 state (C_{2v} symmetry), respectively, showing metal–metal d–d bonding in the anion. The current cluster geometries are in qualitative agreement with prior DFT studies at the PBE level for $M = Cr$ and the B3LYP level for $M = W$. The BP86 and PW91 functionals significantly outperform the B3LYP functional for the Cr species, in terms of relative energies, electron detachment energies, and electronic excitation energies, whereas the B3LYP functional is better for the W species. Accurate heats of formation for the ground states of M_3O_8 are calculated from the clustering energies and the heats of formation of MO_2 and MO_3 . The energetics have been used to predict redox reaction thermochemistry.

1. Introduction

Early transition metal oxides (TMOs) have broad technological applications.¹ Chromium oxides are catalysts for many industrial processes,² and CrO_2 is widely used in magnetic recording tapes and other magnetic media.³ Chromium possesses a half-filled $3d^54s^1$ electronic configuration and various oxidation states which give rise to oxides with different physical and chemical properties. Gas phase chromium oxide clusters with well-defined structures and atomic connectivity and tunable stoichiometries serve as ideal molecular models for mechanistic insight into the complex surface and catalytic processes at a molecular level.⁴ In the gas phase, chromium oxide clusters have received both experimental^{5–20} and theoretical^{14,15,17,18,20–24} attention over the past two decades. The potential for ferromagnetic versus antiferromagnetic spin coupling in the $Cr_2O_n^{0/-}$ ($n = 1–3$) clusters was particularly intriguing, raising the interesting possibility of chemical control of magnetic properties.^{14,19} In a recent work, two families of stable oxide clusters, $Cr_nO_{3n}^{-/0/+}$ and $Cr_nO_{2n+2}^{-/0/+}$, were found from a combination of flow tube reactions and density functional theory (DFT) calculations; each family was predicted to have distinct electronic and magnetic properties.¹⁵ Among the latter series is the $Cr_3O_8^-$ cluster, which was predicted to possess three unpaired spins, reminiscent of the magnetism of the CrO_2 films.³

However, the structural and electronic properties of the $Cr_3O_8^-$ and Cr_3O_8 clusters remain poorly characterized.

We are interested in developing cluster models^{17–20,23–29} for early TMO catalysts and in elucidating new types of chemical bonding in TMO clusters.^{26,30–32} In our prior studies, we characterized three series of chromium oxide clusters, CrO_n^- ($n = 1–5$),¹⁷ $Cr_2O_n^-$ ($n = 1–7$),¹⁹ and $Cr_nO_{3n}^-$ ($n = 1–5$),²⁰ using photoelectron spectroscopy (PES) and electronic structure calculations. Chromium and its complexes are known to be challenging targets for computational chemistry.³³ Synergistic experimental and computational studies on chromium oxide clusters are thus highly desirable to benchmark theoretical methods. In addition, tungsten oxides and clusters are also important catalytically and the tungsten oxide clusters tend to have lower spin states than do the chromium oxide clusters. Thus a comparison between tungsten oxide clusters and chromium oxide clusters provides unique insights into how the cluster property changes with changes in atomic number in a column of the periodic table.

In the current contribution, we report a comparative study of the $M_3O_8^-$ ($M = Cr, W$) anions and their neutrals, which can be considered as reduced species of the well-characterized stoichiometric M_3O_9 ($M = Cr, W$) clusters.^{15,20,23,26,27,32,34} PES spectra are obtained for $M_3O_8^-$ ($M = Cr, W$) at photon energies of 193 nm (6.424 eV) and 157 nm (7.866 eV). Very different overall PES patterns are observed for the Cr versus W species. Extensive DFT and molecular orbital theory (CCSD(T)) calculations were performed to locate the ground and low-lying excited states for the neutrals and anions. The ground states of

* Corresponding authors. E-mail: ls.wang@pnl.gov (L.-S.W.); dadixon@bama.ua.edu (D.A.D.).

[†] The University of Alabama.

[‡] Washington State University and Pacific Northwest National Laboratory.

Cr_3O_8 and Cr_3O_8^- are predicted to be the ${}^3\text{B}_2$ and ${}^4\text{B}_2$ states of a C_{2v} structure, respectively. In contrast, those of W_3O_8 and W_3O_8^- are predicted to be the ${}^1\text{A}'$ state (C_s symmetry) and the ${}^2\text{A}_1$ state (C_{2v} symmetry), respectively. The M_3O_8^- ($\text{M} = \text{Cr}, \text{W}$) cluster geometries are in qualitative agreement with prior DFT studies at the PBE level with a double- ζ basis set for $\text{M} = \text{Cr}$ ¹⁵ and at the B3LYP level with a triple- ζ basis set.²⁷ Ferromagnetic spin coupling is predicted for the ground states of Cr_3O_8 and Cr_3O_8^- , whereas metal–metal d–d bonding is predicted for the ground state of W_3O_8^- . The current combined experimental and theoretical data also benchmark the performance of DFT methods for the Cr and W oxide clusters. The energetic results have been used to predict the energetics of the oxidative dehydrogenation of CH_3OH to probe the potential redox properties of these clusters.

2. Experimental and Computational Methods

2.1. Photoelectron Spectroscopy. The experiment was carried out using a magnetic-bottle PES apparatus equipped with a laser vaporization cluster source, details of which have been described elsewhere.³⁵ Briefly, M_mO_n^- ($\text{M} = \text{Cr}, \text{W}$) clusters were produced by laser vaporization of a pure Cr or W disk target in the presence of a He carrier gas seeded with 0.5% O_2 , and analyzed using a time-of-flight mass spectrometer. The Cr_3O_8^- and W_3O_8^- clusters of current interest were each mass-selected and decelerated before being photodetached. Due to the relatively high electron binding energies, high photon energies were used in the photodetachment experiment: 193 nm (6.424 eV) and 157 nm (7.866 eV). Efforts were made to choose colder clusters (i.e., clusters with long resident times in the nozzle) for photodetachment, which has proved essential for obtaining high-quality PES data.³⁶ Photoelectrons were collected at nearly 100% efficiency by the magnetic bottle and analyzed in a 3.5 m long electron flight tube. PES spectra were calibrated using the known spectrum of Au^- and the energy resolution of the PES apparatus was $\Delta E_k/E_k \sim 2.5\%$, i.e., ~ 25 meV for 1 eV electrons.

2.2. Computational Methods. Equilibrium geometries and vibrational frequencies were calculated at the DFT level with the B3LYP,³⁷ BP86,³⁸ and PW91³⁹ exchange-correlation functionals for both the neutral and anionic clusters to obtain the adiabatic and vertical electron detachment energies (ADEs and VDEs) for the anions. Due to the potential for artificial symmetry breaking with the B3LYP functional for several anionic clusters as found in our recent studies,²⁴ we used the zero-point vibrational energies (ZPEs) calculated at the BP86 level. Our recent benchmark studies on the ADEs and VDEs for the monomers and dimers of the group VIB TMO cluster anions have shown that functionals with Hartree–Fock (HF) exchange (i.e., hybrid functionals) such as B3LYP tend to overestimate the electron detachment energies when there is a potential for significant multireference character, whereas functionals without HF exchange (i.e., pure functionals) such as BP86 and PW91 give better results.²⁴ In these calculations, we used the aug-cc-pVDZ basis set⁴⁰ for O and the aug-cc-pVDZ-PP basis set based on the relativistic effective core potential (RECP) for transition metals;⁴¹ these basis sets will be collectively denoted as aVDZ. The RECP-based basis sets for Cr were constructed in the same manner as those for the second- and third-row transition metal atoms. Single point energy calculations were carried out at the DFT level with these functionals using the aug-cc-pVTZ basis set for O and the aug-cc-pVTZ-PP basis set for Cr and W; these basis sets will be denoted as aVTZ. In addition, single point energies were also calculated with the coupled cluster method at the CCSD(T)⁴²

level with the aVDZ and aVTZ basis sets at the B3LYP/aVDZ geometries. For open-shell systems, the R/UCCSD(T) approach was used, where a restricted open-shell Hartree–Fock (ROHF) calculation was initially performed and the spin constraint was relaxed in the correlation treatment.⁴³ Core–valence correlation corrections were calculated at the CCSD(T) level with the aug-cc-pCVDZ basis set for O⁴⁴ and the aug-cc-pCVDZ-PP basis set for the transition metals; these basis sets will be denoted as awCVDZ. This method follows on the approach developed previously for the accurate prediction of the heats of formation for a wide range of compounds.⁴⁵

The above CCSD(T) and DFT calculations were carried out for the lowest energy state of each spin and spatial symmetry for each trial structure; the electron excitation energies and detachment energies calculated in this manner are denoted as self-consistent energies. In addition, we used the time-dependent DFT (TD-DFT) method⁴⁶ with the above functionals to calculate the lowest few excitation energies from the optimized neutral and anionic ground state geometries for the neutral. An asymptotic correction^{46f,g} for the B3LYP exchange-correlation functional was employed, and no significant effect was observed on the transition energies for these relatively low energy excited states.

The DFT calculations were carried out with the Gaussian 03 program package.⁴⁷ For the pure DFT methods (BP86 and PW91), the density fitting approximation was employed to speed up the calculations.⁴⁸ The density fitting sets were automatically generated from the atomic orbital primitives.⁴⁷ The CCSD(T) calculations were carried out with the MOLPRO 2006.1 program packages.⁴⁹ The TD-DFT calculations were performed with the NWChem 5.1 program packages.⁵⁰ The calculations were carried out on the Opteron-based dense memory cluster (DMC) and Itanium 2-based Altix supercomputers at the Alabama Supercomputer Center, the Xeon-based Dell Linux cluster at the University of Alabama, the local Xeon-based and Opteron-based Penguin Computing Linux clusters, and the Opteron-based Linux cluster in the Molecular Science Computing Facility at the Pacific Northwest National Laboratory.

3. Experimental Results

Figure 1 shows the PES spectra of Cr_3O_8^- at the 193 and 157 nm photon energies. The 193 nm spectrum (Figure 1a) exhibits two intense and relatively sharp bands (X and A). The ground state VDE (4.44 eV; Table 1) was determined from the peak maximum of the leading X band. Because no vibrational structure was resolved, the ground state ADE was determined by drawing a straight line along the leading edge of band X and then adding the instrumental resolution to the intersection with the binding energy axis. Although this was an approximate procedure, we were able to obtain a consistent ADE for band X from the spectra taken at the two different photon energies. The ADE (i.e., the electron affinity of the corresponding Cr_3O_8 neutral species) thus determined is 4.31 eV. Band A (ADE, 4.78 eV; VDE, 4.95 eV) shows a similar bandwidth and intensity relative to band X. The electron signals beyond band A are weak and congested, covering the binding energy regime of 5.2–6.2 eV in the 193 nm spectrum (not labeled).

The 157 nm spectrum (Figure 1b) further reveals intense bands beyond 6 eV, which are labeled “B”, “C”, and “D”. Bands B (6.47 eV) and D (7.69 eV) are sharp and well-resolved, whereas band C covers a regime of 6.7–7.2 eV, probably containing multiple overlapping electronic states. Note that the

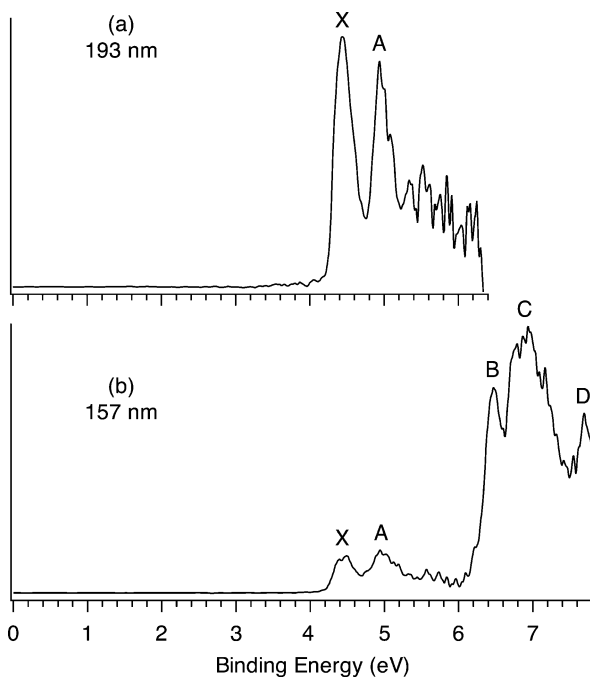


Figure 1. Photoelectron spectra of $Cr_3O_8^-$ at (a) 193 nm (6.424 eV) and (b) 157 nm (7.866 eV).

TABLE 1: Observed Adiabatic (ADE) and Vertical (VDE) Electron Detachment Energies from the Photoelectron Spectra of $Cr_3O_8^-$ and $W_3O_8^-$

cluster	feature	ADE ^a (eV)	VDE ^a (eV)
$Cr_3O_8^-$	X	4.31(3) ^b	4.44(3)
	A	4.78(5)	4.95(5)
	B	6.30(5)	6.47(3)
	C	—	6.7–7.2
	D	—	7.69(2)
$W_3O_8^-$	X	4.37(5) ^b	4.62(5)
	A	6.65(3)	6.78(3)
	B	—	7.23(5)
	C	—	7.65(5)

^a Numbers in parentheses represent the experimental uncertainty in the last digit. ^b Electron affinity of the corresponding neutral species.

higher binding energy bands (B, C, and D) all show significant higher intensities relative to the lower binding energy bands (X and A).

The 157 nm spectrum of $W_3O_8^-$ was presented in a previous paper on the $W_3O_n^-$ ($n = 7–10$) series²⁷ and is included here for completeness (Figure 2b). The 193 nm spectrum (Figure 2a) displays only a single ground state band X (ADE, 4.37 eV; VDE, 4.62 eV). At 157 nm (Figure 2b), band X is followed by a large energy gap (2.28 eV as evaluated from the ADE difference) and three well-defined bands at higher binding energies: A (ADE, 6.65 eV; VDE, 6.78 eV), B (VDE, 7.23 eV), and C (VDE, 7.65 eV). All the observed electron binding energies for the two $M_3O_8^-$ species are given in Table 1.

4. Computational Results

The M_3O_8 ($M = Cr, W$) cluster can be derived from the M_3O_9 cluster^{15,20,23,26,27,32,34} by removing one oxygen atom. Four types of structures were studied in the current calculations, as shown in Figure 3. Our recent studies predicted the ground state of M_3O_9 to be the ring structure (Figure S1, Supporting Information), where the six-membered ring is puckered for $M = Cr$

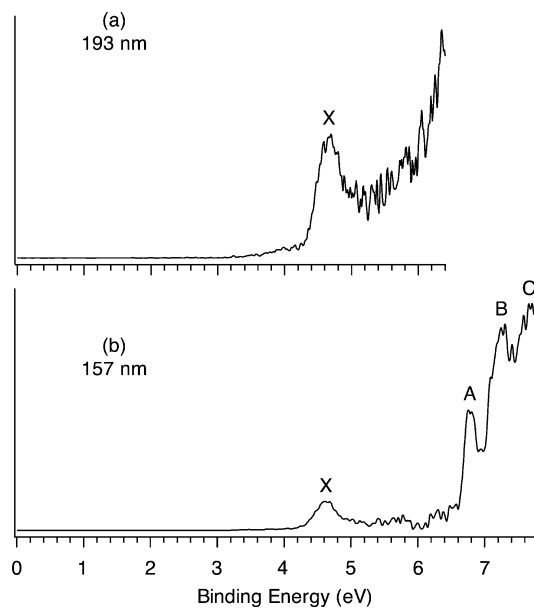


Figure 2. Photoelectron spectra of $W_3O_8^-$ at (a) 193 nm and (b) 157 nm.

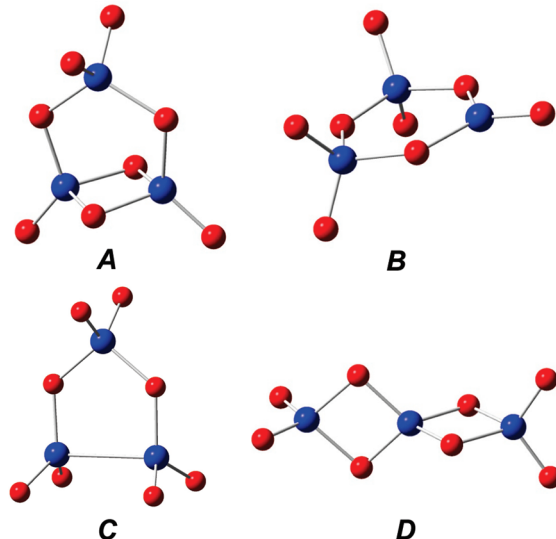


Figure 3. Molecular structures of the M_3O_8 and $M_3O_8^-$ ($M = Cr, W$) clusters.

and planar for $M = W$.^{20,23,26,27} Assuming the cluster structure is not significantly changed by removing one oxygen atom, one arrives at structures **B** and **C** by removing one terminal and one bridge oxygen atom, respectively. Structure **A** can be obtained from structure **B** by rotating an MO_2 group to convert a terminal oxygen atom into a bridge oxygen atom. Structure **A** was proposed by Bergeron et al.¹⁵ as the ground states of Cr_3O_8 and its anion. We previously predicted that the chain structure of M_3O_9 (Figure S1, Supporting Information) is ~ 34 and 25 kcal/mol higher in energy than its ring structure at the B3LYP/aVTZ//B3LYP/aVDZ level for $M = Cr$ and W , respectively.²³ Structure **D** for M_3O_8 can be obtained from the chain structure of M_3O_9 by removing the terminal oxygen atom from the central metal atom.

Structures of the low-lying excited electronic states calculated at the B3LYP/aVDZ level with single point energies at the CCSD(T)/aVDZ level are given in Figure 4 for Cr_3O_8 , in Figure 5 for $Cr_3O_8^-$, in Figure 6 for W_3O_8 , and in Figure 7 for $W_3O_8^-$. Electronic energies of most of these structures were also

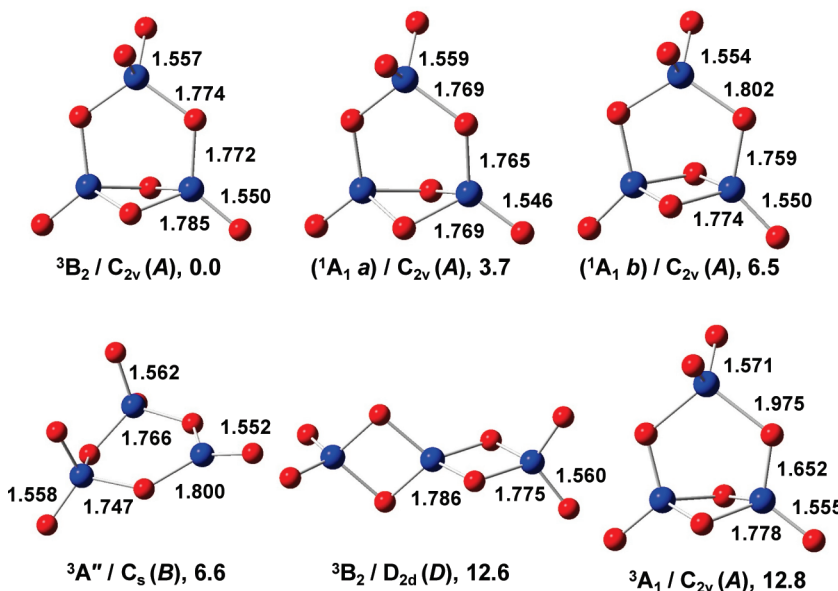


Figure 4. Low-lying electronic states of Cr_3O_8 calculated at the CCSD(T)/aVDZ//B3LYP/aVDZ level. Relative energies are given in kcal/mol.

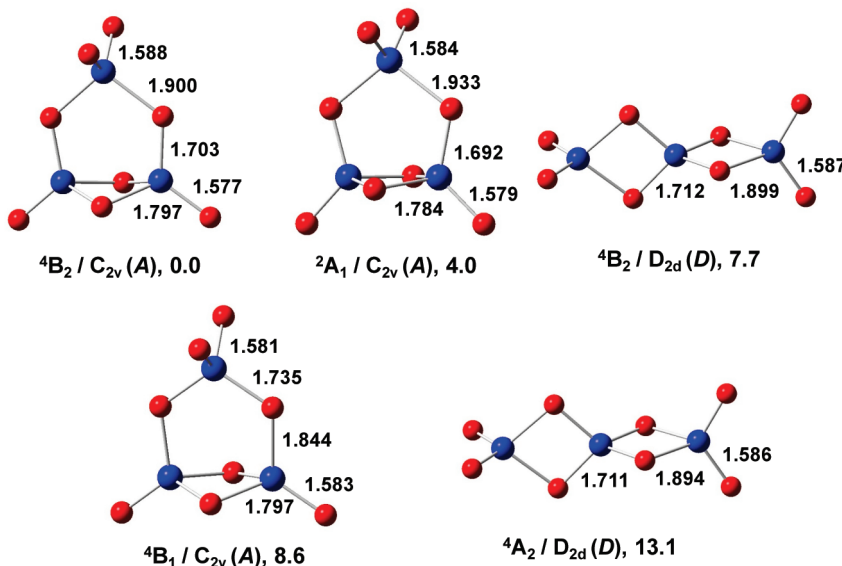


Figure 5. Low-lying electronic states of Cr_3O_8^- calculated at the CCSD(T)/aVDZ//B3LYP/aVDZ level. Relative energies are given in kcal/mol.

calculated at the CCSD(T)/aVTZ level with the core–valence corrections calculated at the CCSD(T)/awCVTZ level. Relative energies calculated at the various levels of theory are listed in Table 2 for $M = \text{Cr}$ and in Table 3 for $M = \text{W}$. Additional higher energy structures together with their relative energies are given as Supporting Information (Figures S2–S5). Electron detachment energies (ADEs and VDEs) for the ground state and numerous excited states were calculated at DFT and CCSD(T) levels as shown in Tables 4, 5, and 6. The relative energies between the quintet and triplet excited states for structure A of Cr_3O_8 and the triplet and open-shell singlet states for structure C of W_3O_8 at the anion geometries are shown in Table 7. Excitation energies were also calculated at the TD-DFT level at the anion ground state geometries, as shown in Table 8.

4.1. Cr_3O_8 . The ground state of Cr_3O_8 (Figure 4) was predicted to be the $^3\text{B}_2$ state of structure A with C_{2v} symmetry. It was consistently calculated as the lowest energy state at the CCSD(T), B3LYP, BP86, and PW91 levels (Table 2). At the CCSD(T)/aVDZ level, five additional low-lying structures were

predicted to lie within 15 kcal/mol from the ground state: the $(^1\text{A}_1 \text{a})$, $(^1\text{A}_1 \text{b})$, and $^3\text{A}_1$ states of structure A also with C_{2v} symmetry, the $^3\text{A}''$ state of structure B with C_s symmetry, and the $^3\text{B}_2$ state of structure D with D_{2d} symmetry. The $(^1\text{A}_1 \text{a})$ and $(^1\text{A}_1 \text{b})$ states of structure A have different highest occupied molecular orbitals (HOMOs).

The ground state structure of Cr_3O_8 has four terminal $\text{Cr}=\text{O}$ bonds of $\sim 1.55 \text{ \AA}$ and eight bridge $\text{Cr}-\text{O}$ bonds of $\sim 1.78 \text{ \AA}$ at the B3LYP/aVDZ level with little variation in each group. These metal–oxygen bond lengths are comparable to those for the ring structure of Cr_3O_9 with terminal $\text{Cr}=\text{O}$ bonds of $\sim 1.55 \text{ \AA}$ and bridge $\text{Cr}-\text{O}$ bonds of $\sim 1.76 \text{ \AA}$ at the same level of theory.²³

4.2. Cr_3O_8^- . The ground state of Cr_3O_8^- is predicted to be the $^4\text{B}_2$ state of structure A with C_{2v} symmetry (Table 2). The $^2\text{A}'$ state of structure B with C_s symmetry (Figure S3 and Table S1, Supporting Information) is predicted to be lower by 5.8 kcal/mol at the CCSD(T)/aVDZ level but has a very large T_1 diagnostic of ~ 0.13 at this level, showing that a single reference wave function is inappropriate and that the overall wave function

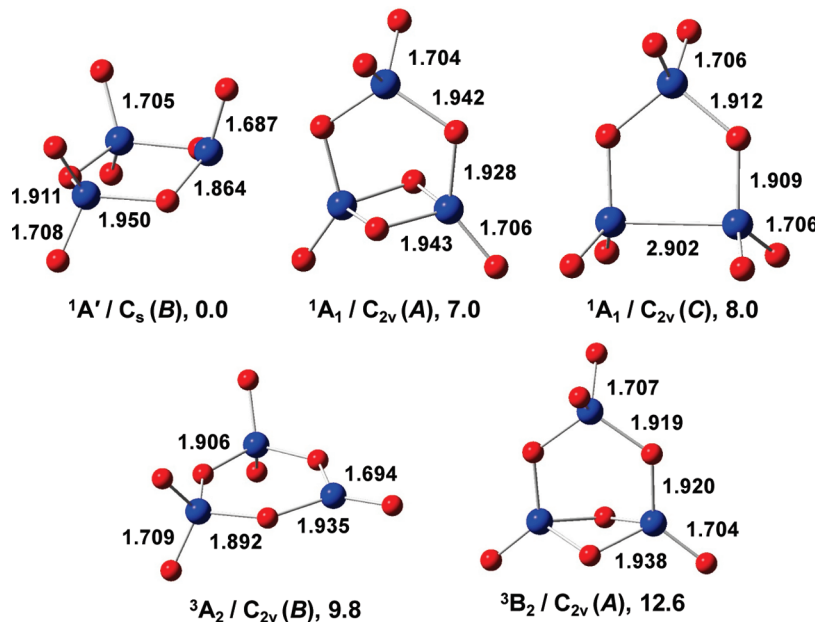


Figure 6. Low-lying electronic states of W_3O_8 calculated at the CCSD(T)/aVDZ//B3LYP/aVDZ level. Relative energies are given in kcal/mol.

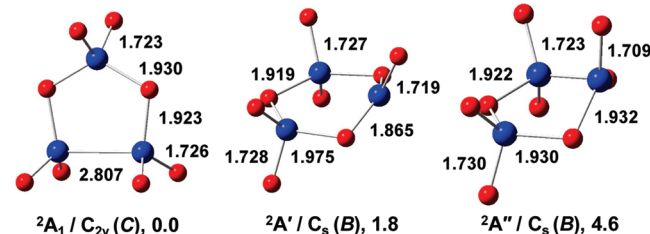


Figure 7. Low-lying electronic states of $W_3O_8^-$ calculated at the CCSD(T)/aVDZ//B3LYP/aVDZ-PP level. Relative energies are given in kcal/mol.

TABLE 2: Relative Energies at 0 K in kcal/mol Calculated at the CCSD(T), B3LYP, BP86, and PW91 Levels for the Low-Lying Electronic States of Cr_3O_8 and $Cr_3O_8^-$

state	CCSD(T)			B3LYP	BP86	PW91
	aVDZ ^b	aVTZ ^c	aVTZ+CV ^d	aVTZ ^e	aVTZ ^f	aVTZ ^g
Cr_3O_8						
$^3B_2/C_{2v}(A)$	0.0	0.0	0.0	0.0	0.0	0.0
$(^1A_1\ a)/C_{2v}(A)$	3.7	3.4	8.7	33.4	15.6	15.8
$(^1A_1\ b)/C_{2v}(A)$	6.5	6.0	7.1	29.2	9.5	9.5
$^3A''/Cs(B)$	6.6	—	—	11.8	13.1	13.2
$^3B_2/D_{2d}(D)$	12.6	14.2	14.3	15.4	9.2	9.8
$^3A_1/C_{2v}(A)$	12.8	13.8	14.0	23.0	14.4	14.6
$Cr_3O_8^-$						
$^4B_2/C_{2v}(A)$	0.0	0.0	0.0	0.0	0.0	0.0
$^2A_1/C_{2v}(A)$	4.0	3.4	4.2	25.5	6.4	6.5
$^4B_2/D_{2d}(D)$	7.7	9.1	9.2	10.7	5.3	5.9
$^4B_1/C_{2v}(A)$	8.6	7.7	8.0	10.1	0.6	0.2
$^4A_2/D_{2d}(D)$	13.1	13.4	13.2	13.6	-2.2	-2.1

^a ZPE corrections at the BP86/aVDZ level. ^b CCSD(T)/aVDZ//B3LYP/aVDZ. ^c CCSD(T)/aVTZ//B3LYP/aVDZ. ^d CCSD(T)/aVTZ//B3LYP/aVDZ with core-valence corrections calculated at the CCSD(T)/awCVDZ//B3LYP/aVDZ level. ^e B3LYP/aVTZ//B3LYP/aVDZ. ^f BP86/aVTZ//BP86/aVDZ. ^g PW91/aVTZ//PW91/aVDZ.

is not being properly described. The $^2A'$ state of structure **B** was predicted to lie substantially higher in energy than the 4B_2 state of structure **A** by 43.7, 20.1, and 20.9 kcal/mol at the B3LYP/aVTZ, BP86/aVTZ, and PW91/aVTZ levels, respectively. Although the 4A_2 state of structure **D** with D_{2d} symmetry was predicted to be ~2 kcal/mol lower in energy than the 4B_2 state of structure **A** at the BP86/aVTZ and PW91/aVTZ levels,

TABLE 3: Relative Energies at 0 K (kcal/mol) Calculated at the CCSD(T), B3LYP, BP86, and PW91 Levels for the Low-Lying Electronic States of W_3O_8 and $W_3O_8^-$

state	CCSD(T)			B3LYP	BP86	PW91
	aVDZ ^b	aVTZ ^c	aVTZ+CV ^d	aVTZ ^e	aVTZ ^f	aVTZ ^g
W_3O_8						
$^1A'/Cs(B)$	0.0	0.0	0.0	0.0	0.0	0.0
$^1A_1/C_{2v}(A)$	7.0	8.6	7.4	14.2	9.8	9.1
$^1A_1/C_{2v}(C)$	8.0	8.7	9.4	9.6	8.9	9.6
$^3A_2/C_{2v}(B)$	9.8	10.1	11.3	5.6	12.9	13.2
$^3B_2/C_{2v}(A)$	12.6	14.5	13.8	12.6	16.1	16.0
$W_3O_8^-$						
$^2A_1/C_{2v}(C)$	0.0	0.0	0.0	0.0	0.0	0.0
$^2A'/Cs(B)$	1.8	1.2	—	2.5	4.5	4.0
$^2A''/Cs(B)$	4.6	4.0	—	4.0	7.4	6.9

^a ZPE corrections at the BP86/aVDZ level. ^b CCSD(T)/aVDZ//B3LYP/aVDZ. ^c CCSD(T)/aVTZ//B3LYP/aVDZ. ^d CCSD(T)/aVTZ//B3LYP/aVDZ with core-valence corrections calculated at the CCSD(T)/awCVDZ//B3LYP/aVDZ level. ^e B3LYP/aVTZ//B3LYP/aVDZ. ^f BP86/aVTZ//BP86/aVDZ. ^g PW91/aVTZ//PW91/aVDZ.

the $^4A_2(D)$ state was predicted to be ~13 kcal/mol higher in energy than the $^4B_2(A)$ state at the CCSD(T)/aVTZ and B3LYP/aVTZ levels. A similar situation occurs for the $^4B_1(A)$ state (Table 2) and the $^2A_1(D)$ state (Table S1, Supporting Information), which were predicted to lie very close in energy to the $^4B_2(A)$ state at the BP86/aVTZ and PW91/aVTZ levels. However, at the CCSD(T)/aVTZ and B3LYP/aVTZ levels, these two states were predicted to be ~10 and 20 kcal/mol higher in energy than the $^4B_2(A)$ state, respectively. At the CCSD(T)/aVDZ level, two additional states were predicted to lie within 15 kcal/mol of the ground state (Figure 5), the $^2A_1(A)$ state, and the $^4B_2(D)$ state.

Compared to the ground state structure of Cr_3O_8 (Figure 4), the ground state structure of $Cr_3O_8^-$ (Figure 5) was predicted to have similar terminal Cr=O bond lengths within 0.04 Å. However, the bridge Cr–O bonds in the anion between the metal center with two terminal Cr=O bonds and the metal centers with only one terminal Cr=O bond were predicted to have substantially different bond lengths than those in the neutral cluster, with two of them elongated by ~0.13 Å and two

TABLE 4: Adiabatic and Vertical Electron Detachment Energies (ADEs and VDEs in eV) Calculated at the CCSD(T), B3LYP, BP86, and PW91 Levels for the Low-Lying Structures of Cr_3O_8^- , Compared to the Experimental Electron Detachment Energies for the X Band^a

transition	orbital ^b	CCSD(T)			B3LYP	BP86	PW91	
		aVDZ ^c	aVTZ ^d	aVTZ+CV ^e	aVTZ ^f	aVTZ ^g	aVTZ ^h	exptl
ADEs								
$^4\text{B}_2 \rightarrow {}^3\text{B}_2/\text{C}_{2v}$ (A)	23a ₁	4.22	4.25	4.24	4.58	3.94	3.89	4.31(3)
$^2\text{A}_1 \rightarrow {}^3\text{B}_2/\text{C}_{2v}$ (A)	<i>i</i>	4.05	4.10	4.06	3.48	3.66	3.61	
$^2\text{A}_1 \rightarrow ({}^1\text{A}_1 \text{ b})/\text{C}_{2v}$ (A)	23a ₁	4.33	4.36	4.36	4.74	4.08	4.03	
$^4\text{B}_1 \rightarrow {}^3\text{B}_2/\text{C}_{2v}$ (A)	6a ₂	3.85	3.92	3.89	4.14	3.92	3.88	
$^4\text{B}_2 \rightarrow {}^3\text{B}_2/\text{D}_{2d}$ (D)	13a ₁	4.44	4.47	4.46	4.79	4.11	4.06	
$^4\text{A}_2 \rightarrow {}^3\text{B}_2/\text{D}_{2d}$ (D)	3b ₁	4.20	4.29	4.29	4.66	4.44	4.41	
VDEs								
$^4\text{B}_2 \rightarrow {}^3\text{B}_2/\text{C}_{2v}$ (A)	23a ₁	4.67	4.75	4.76	5.16	4.24	4.19	4.44(3)
$^2\text{A}_1 \rightarrow {}^3\text{B}_2/\text{C}_{2v}$ (A)	<i>i</i>	5.58	5.68	5.62	5.14	4.91	4.88	
$^2\text{A}_1 \rightarrow ({}^1\text{A}_1 \text{ b})/\text{C}_{2v}$ (A)	23a ₁	4.86	4.94	4.94	5.30	4.38	4.34	
$^4\text{B}_1 \rightarrow {}^3\text{B}_2/\text{C}_{2v}$ (A)	6a ₂	4.02	4.13	4.12	4.42	4.05	4.02	
$^4\text{B}_2 \rightarrow {}^3\text{B}_2/\text{D}_{2d}$ (D)	13a ₁	4.81	4.89	4.92	5.46	4.32	4.28	
$^4\text{A}_2 \rightarrow {}^3\text{B}_2/\text{D}_{2d}$ (D)	3b ₁	4.61	4.74	4.78	5.34	4.67	4.65	

^a ZPE corrections for the ADE at the BP86/aVDZ level. ^b The molecular orbital where the electron is removed. The electron configuration at the BP86/aVDZ level for the $^4\text{B}_2$ state of structure **A** is ... $(22\text{a}_1)^1(15\text{b}_2)^1(23\text{a}_1)^1$. That for the $^2\text{A}_1$ state of structure **A** is ... $(23\text{a}_1)^1$. That for the $^4\text{B}_1$ state of structure **A** is ... $(15\text{b}_2)^1(22\text{a}_1)^1(6\text{a}_2)^1$. That for the $^4\text{B}_2$ state of structure **D** is ... $(12\text{b}_2)^1(12\text{a}_1)^1(13\text{a}_1)^1$. That for the $^4\text{A}_2$ state of structure **D** is ... $(12\text{b}_2)^1(12\text{a}_1)^1(3\text{b}_1)^1$. ^c CCSD(T)/aVDZ//B3LYP/aVDZ. ^d CCSD(T)/aVTZ//B3LYP/aVDZ. ^e CCSD(T)/aVTZ//B3LYP/aVDZ with core-valence corrections calculated at the CCSD(T)/awCVDZ//B3LYP/aVDZ level. ^f B3LYP/aVTZ//B3LYP/aVDZ. ^g BP86/aVTZ//BP86/aVDZ. ^h PW91/aVTZ//PW91/aVDZ. ⁱ Transitions involve orbital relaxation.

TABLE 5: Adiabatic and Vertical Electron Detachment Energies (ADEs and VDEs in eV) Calculated at the CCSD(T), B3LYP, BP86, and PW91 Levels for the Low-Lying Structures of W_3O_8^- , Compared to the Experimental Electron Detachment Energies for the X Band^a

transition	orbital ^b	CCSD(T)			B3LYP	BP86	PW91	
		aVDZ ^c	aVTZ ^d	aVTZ+CV ^e	aVTZ ^f	aVTZ ^g	aVTZ ^h	exptl
ADEs								
$^2\text{A}_1 \rightarrow {}^1\text{A}_1/\text{C}_{2v}$ (C)	20a ₁	3.77	3.75	3.86	3.90	4.06	4.02	4.37(5)
$^2\text{A}' \rightarrow {}^1\text{A}'/\text{C}_s$ (B)	32a'	3.34	3.35	—	3.37	3.48	3.43	
$^2\text{A}'' \rightarrow {}^1\text{A}'/\text{C}_s$ (B)	23a''	3.22	3.22	—	3.31	3.35	3.31	
VDEs								
$^2\text{A}_1 \rightarrow {}^1\text{A}_1/\text{C}_{2v}$ (C)	20a ₁	4.31	4.41	4.45	4.66	4.65	4.62	4.62(5)
$^2\text{A}' \rightarrow {}^1\text{A}'/\text{C}_s$ (B)	32a'	3.73	3.84	—	4.07	3.96	3.92	
$^2\text{A}'' \rightarrow {}^1\text{A}'/\text{C}_s$ (B)	23a''	3.61	3.73	—	3.95	3.88	3.84	

^a ZPE corrections for the ADE at the BP86/aVDZ level. ^b The molecular orbital where the electron is removed. The electron configuration at the B3LYP/aVDZ level for the $^2\text{A}_1$ state of structure **C** is ... $(20\text{a}_1)^1$. That for the $^2\text{A}'$ state of structure **B** is ... $(32\text{a}')^1$. That for the $^2\text{A}''$ state of structure **B** is ... $(23\text{a}'')^1$. ^c CCSD(T)/aVDZ//B3LYP/aVDZ. ^d CCSD(T)/aVTZ//B3LYP/aVDZ. ^e CCSD(T)/aVTZ//B3LYP/aVDZ with core-valence corrections calculated at the CCSD(T)/awCVDZ//B3LYP/aVDZ level. ^f B3LYP/aVTZ//B3LYP/aVDZ. ^g BP86/aVTZ//BP86/aVDZ. ^h PW91/aVTZ//PW91/aVDZ.

shortened by ~ 0.07 Å. The other bridge Cr–O bonds were predicted to have rather similar bond lengths in the neutral and anionic clusters.

4.3. W_3O_8 . The ground state of W_3O_8 was predicted to be the ${}^1\text{A}'$ state of structure **B** with C_s symmetry at the various levels of theory (Figure 6 and Table 3), and it is different in structure from the ground state of Cr_3O_8 . At the CCSD(T)/aVDZ level, four additional low-lying structures were predicted to lie within 15 kcal/mol of the ground state, the ${}^1\text{A}_1$ and ${}^3\text{B}_2$ states of structure **A**, the ${}^3\text{A}_2$ state of structure **B**, and the ${}^1\text{A}_1$ state of structure **C**.

The ground state structure of W_3O_8 was predicted to have five terminal W=O bonds of ~ 1.70 Å and six bridge W–O bonds of $1.85\text{--}1.95$ Å at the B3LYP/aVDZ level, consistent with our previous calculations at the same level.²⁷ The two bridge W–O bonds on the metal center with only one terminal W=O bond are shorter than those on the other two metal centers. These bond lengths can be compared to those calculated for the ring structure of W_3O_9 at the same level of theory: ~ 1.71 Å for the terminal W=O bonds and ~ 1.91 Å for the bridge

W–O bonds.³² The six-membered ring in the ground state of W_3O_8 is nonplanar in contrast to the planar ring in the ground state of W_3O_9 (Table S1, Supporting Information).

4.4. W_3O_8^- . As shown in Figure 7 and Table 3, the ground state of W_3O_8^- was consistently predicted to be the ${}^2\text{A}_1$ state of structure **C** with C_{2v} symmetry at the CCSD(T), B3LYP, BP86, and PW91 levels. Our previous B3LYP calculations reached the same ground state for W_3O_8^- .²⁷ The ${}^2\text{A}'$ and ${}^2\text{A}''$ states of structure **B** were predicted to lie ~ 2 and 5 kcal/mol above the ground state, respectively. Compared to the ${}^1\text{A}_1$ state of structure **C** of W_3O_8 , the ${}^2\text{A}_1$ state of structure **C** of W_3O_8^- has similar metal–oxygen bond lengths but a shorter W–W bond length.

5. Comparison between Experiment and Theory

Tables 4 and 5 compare the calculated ADEs and VDEs for a variety of anionic and neutral isomers and states with the experimental values for the X bands of Cr_3O_8^- and W_3O_8^- . Due to the presence of two isomers each with up to three low-lying electronic states for the anionic clusters and up to three isomers

TABLE 6: Adiabatic and Vertical Electron Detachment Energies (ADEs and VDEs in eV) to the Excited States of the Neutral Cluster Calculated at the CCSD(T), B3LYP, BP86, and PW91 Levels for the Ground State of $Cr_3O_8^-$ and $W_3O_8^-$, Compared to the Experimental Electron Detachment Energies for the Higher Energy Bands^a

transition	orbital ^b	CCSD(T) ^c			B3LYP ^c	BP86 ^c	PW91 ^c	exptl
		aVDZ ^d	aVTZ ^e	aVTZ+CV ^f	aVTZ ^g	aVTZ ^h	aVTZ ⁱ	
$Cr_3O_8^-$, ADEs								
$^4B_2 \rightarrow ^3A_1/C_{2v}$ (A)	15b ₂	4.78	4.85	4.85	5.58	4.57	4.52	4.78(5) (A)
$^4B_2 \rightarrow ^5A_2/C_{2v}$ (A)	12b ₁	6.20	6.28	6.30	6.18	5.91	5.87	6.30(5) (B)
$^4B_2 \rightarrow ^5A_1/C_{2v}$ (A)	14b ₂	6.78	6.88	6.90	6.77	6.41	6.37	
$^4B_2 \rightarrow ^5B_2/C_{2v}$ (A)	21a ₁	6.75	6.89	6.94	7.12	6.54	6.50	
$^4B_2 \rightarrow ^5B_1/C_{2v}$ (A)	5a ₂	7.17	7.28	7.29	7.27	6.84	6.80	
$Cr_3O_8^-$, VDEs								
$^4B_2 \rightarrow ^3A_1/C_{2v}$ (A)	15b ₂	5.16	5.24	5.26	6.04	4.95	4.91	4.95(5) (A)
$^4B_2 \rightarrow ^5A_2/C_{2v}$ (A)	12b ₁	6.60	6.73	6.73 (6.75)	6.48 (6.49)	6.05 (6.06)	6.01 (6.02)	6.47(3) (B)
$^4B_2 \rightarrow ^5A_1/C_{2v}$ (A)	14b ₂	7.07	7.22	7.24 (7.25)	7.09	6.56	6.52	6.7–7.2 (C)
$^4B_2 \rightarrow ^5B_2/C_{2v}$ (A)	21a ₁	6.87	7.00	7.04 (7.07)	7.23	6.59	6.55	
$^4B_2 \rightarrow ^5B_1/C_{2v}$ (A)	5a ₂	7.43	7.56	7.56 (7.59)	7.59 (7.51)	7.05 (7.05)	7.01 (7.01)	7.69(2) (D)
$W_3O_8^-$, ADEs								
$^2A_1 \rightarrow ^3A_1/C_{2v}$ (C)	19a ₁	6.41	6.44	6.54	6.39	6.17	6.16	6.65(3) (A)
$^2A_1 \rightarrow ^3A_2/C_{2v}$ (C)	8a ₂	6.92	7.02	7.03	6.84	6.35	6.30	
$^2A_1 \rightarrow ^3B_1/C_{2v}$ (C)	12b ₁	6.85	6.98	6.99	6.90	6.50	6.45	
$^2A_1 \rightarrow (^3B_2\ b)/C_{2v}$ (C)	14b ₂	7.57	7.68	7.69	7.42	6.79	6.75	
$W_3O_8^-$, VDEs								
$^2A_1 \rightarrow ^3A_1/C_{2v}$ (C)	19a ₁	6.61	6.70	6.76 (7.38)	6.76	6.49	6.45	6.78(3) (A)
$^2A_1 \rightarrow ^3A_2/C_{2v}$ (C)	8a ₂	7.12	7.23	7.24 (7.32)	7.04 (7.05)	6.49 (6.51)	6.45 (6.46)	7.23(5) (B)
$^2A_1 \rightarrow (^3B_1\ a)/C_{2v}$ (C)	12b ₁	7.28	7.39	7.40 (7.70)	7.09 (7.10)	6.83	7.01	7.65(5) (C)
$^2A_1 \rightarrow (^3B_2\ b)/C_{2v}$ (C)	14b ₂	7.85	7.96	7.98 (8.12)	7.51 (7.59)	6.89 (6.93)	6.84 (6.89)	

^a ZPE corrections at the BP86/aVDZ level. ^b The molecular orbital where the electron is removed. The electron configuration at the BP86/aVDZ level for the 4B_2 state of structure **A** of $Cr_3O_8^-$ is $\dots(5a_2)^2(10b_1)^2(21a_1)^2(14b_2)^2(11b_1)^2(12b_1)^2(22a_1)^1(15b_2)^1(23a_1)^1$. That at the B3LYP/aVDZ level for the 2A_1 state of structure **C** of $W_3O_8^-$ is $\dots(14b_2)^2(11b_1)^2(12b_1)^2(8a_2)^2(19a_1)^2(20a_1)^1$. ^c Numbers in the parentheses are for the corresponding low spin states (triplets for $M = Cr$ and open-shell singlets for $M = W$). See text. ^d CCSD(T)/aVDZ//B3LYP/aVDZ. ^e CCSD(T)/aVTZ//B3LYP/aVDZ. ^f CCSD(T)/aVTZ//B3LYP/aVDZ with core-valence corrections calculated at the CCSD(T)/awCVDZ//B3LYP/aVDZ level. ^g B3LYP/aVTZ//B3LYP/aVDZ. ^h BP86/aVTZ//BP86/aVDZ. ⁱ PW91/aVTZ//PW91/aVDZ.

TABLE 7: Relative Energies in kcal/mol between the Quintet and Triplet States for Structure **A** of Cr_3O_8 and the Triplet and Open Shell Singlet States for Structure **C** of W_3O_8 at the Anion Geometries^a

Cr_3O_8/C_{2v} (A)	ΔE	W_3O_8/C_{2v} (C)	ΔE
$E(^3A_2)-E(^5A_2)$	0.4	$E(^1A_1)-E(^3A_1)$	14.2
$E(^3A_1)-E(^5A_1)$	0.3	$E(^1A_2)-E(^3A_2)$	1.7
$E(^3B_2)-E(^5B_2)$	0.7	$E(^1B_1\ a)-E(^3B_1\ a)$	6.8
$E(^3B_1)-E(^5B_1)$	0.6	$E(^1B_2\ b)-E(^3B_2\ b)$	3.2

^a Electronic energies of the high spin states were calculated at the ROHF/aVDZ//B3LYP/aVDZ level, and those of the low spin states were calculated at the CASSCF/aVDZ//B3LYP/aVDZ level. See text.

with up to four electronic states for the neutral clusters, we have calculated the ADE and VDE for each allowed transition from these structures/low-lying electronic states of the anion to the lowest-lying electronic state(s) of the neutral cluster of the same structure. Table 6 compares the calculated ADEs and VDEs for the excited states with the experimental observations. ADEs and VDEs calculated for additional transitions to higher energy structures/states of the neutral are given as Supporting Information (Tables S3–S5).

5.1. The X Band of $Cr_3O_8^-$. For $Cr_3O_8^-$, the ground state (the 4B_2 state of structure **A**) has an electron configuration of $\dots(5a_2)^2(10b_1)^2(21a_1)^2(14b_2)^2(11b_1)^2(12b_1)^2(22a_1)^1(15b_2)^1(23a_1)^1$ at the BP86/aVDZ level (Figure 8). Removal of an electron from its singly occupied molecular orbitals (SOMOs) leads to the 3B_2 and 3A_1 states of the neutral. The ADE and VDE for the transition from the ground state of the anion, 4B_2 (structure **A**), to the ground state of the neutral cluster, 3B_2 (structure **A**), were calculated to be 4.24 and 4.76 eV at the CCSD(T)/aVTZ

level (Table S3, Supporting Information). These can be compared with the experimental values for the X band of 4.31 and 4.44 eV, respectively. The ADE is in better agreement than the VDE, consistent with our recent benchmark study on the electron detachment energies of the MO_3^- and $M_2O_6^-$ ($M = Cr, Mo, W$) clusters, where the calculated ADEs at the CCSD(T)/aVTZ level for $M = Cr$ are in excellent agreement with the experimental values within 0.05 eV, and the calculated VDEs are larger than the experimental values by ~0.1 and 0.2 eV for the monomer and dimer, respectively.²⁴ The ADE and VDE for this transition calculated at the CCSD(T)/aVDZ level are smaller by <0.1 eV than those calculated at the CCSD(T)/aVTZ level, and the core–valence corrections calculated at the CCSD(T)/awCVDZ level are negligible.

The calculated ADE and VDE for the $^2A' \rightarrow ^3A''$ transition at the CCSD(T) level are substantially larger than the experimental values by 0.4–0.5 eV (Table 4) and the $^2A'$ state of structure **B** is ruled out as the ground state. The calculated ADE and VDE at the CCSD(T) level for the $^4B_1 \rightarrow ^3B_2$ transition of structure **A** are smaller than the experimental values by 0.3–0.4 eV, and thus, the 4B_1 state of structure **A** can be ruled out as well. The higher energy 4B_2 (**D**) state and the 2A_1 (**A**) state have VDEs at the CCSD(T) level larger than the experimental value by ~0.5 eV, consistent with the fact that these states are not present in the experiment. In addition, one of the transitions ($^2A_1 \rightarrow ^3B_2$ of structure **A**) listed in Table 4 and some of the transitions included as Supporting Information (Tables S3–S5) cannot be described by one-electron processes.

The $^4A_2 \rightarrow ^3B_2$ transition of structure **D** is comparable to the $^4B_2 \rightarrow ^3B_2$ transition of structure **A** in terms of the ADE and VDE at the CCSD(T) level (Table 4). The 4A_2 state of structure

TABLE 8: Excitation Energies in eV of $M_3O_8^-$ ($M = Cr, W$) Calculated at the TD-DFT Level with the B3LYP/aVDZ, BP86/aVDZ, and PW91/aVDZ Methods at the Ground State Geometries of the Anion, Compared with Those Calculated Self-Consistently at the CCSD(T)/aVDZ//B3LYP/aVDZ, B3LYP/aVTZ//B3LYP/aVDZ, BP86/aVTZ//BP86/aVDZ, and PW91/aVTZ//PW91/aVDZ Levels, and the Experimental Vertical Electron Detachment Energy Differences (ΔE_{vert}^a)^a

excitation	orbital ^b	TD-DFT ^c			ΔE_{vert}^c				ΔE_{vert} exptl
		B3LYP ^d	BP86 ^e	PW91 ^f	CCSD(T) ^g	B3LYP ^h	BP86 ⁱ	PW91 ^j	
$Cr_3O_8, {}^3B_2/C_{2v}$ (A)									
${}^3B_2 \rightarrow {}^3A_1$	$15b_2 \rightarrow 23a_1$	1.19	0.56	0.55	0.49	0.88	0.71	0.72	0.51(5) (A)
${}^3B_2 \rightarrow ({}^3B_2 b)^k$	$22a_1 \rightarrow 23a_1$	0.99	0.65	0.64	—	—	—	—	—
${}^3B_2 \rightarrow ({}^3B_1 a)$	$(22a_1 \rightarrow 6a_2)$	1.00	0.92	0.90	1.05	1.33	0.85	0.85	—
${}^3B_2 \rightarrow ({}^3A_2 a)$	$(15b_2 \rightarrow 6a_2)$	2.39	1.02	1.00	1.29	1.72	1.01	1.00	—
${}^3B_2 \rightarrow ({}^3A_2 b)$	$(22a_1 \rightarrow 13b_1)$	1.10	1.46	1.44	1.32	1.78	1.28	1.28	—
${}^3B_2 \rightarrow ({}^3B_1 b)$	$(15b_2 \rightarrow 13b_1)$	2.51	1.50	1.48	1.56	1.77	1.34	1.34	—
${}^3B_2 \rightarrow ({}^3B_1 c)^k$	$(22a_1 \rightarrow 7a_2)$	2.21	1.71	1.70	—	—	—	—	—
${}^3B_2 \rightarrow ({}^3A_1 b)$	$(22a_1 \rightarrow 16b_2)$	2.12	1.78	1.78	1.73	1.98	1.91	1.91	—
${}^3B_2 \rightarrow ({}^3A_2 c)^k$	$(15b_2 \rightarrow 7a_2)$	2.61	1.82	1.82	—	—	—	—	—
${}^3B_2 \rightarrow {}^5A_2$	$12b_1 \rightarrow 23a_1$	(1.91)	(1.87)	(1.87)	1.93 (1.95)	1.31 (1.33)	1.81 (1.82)	1.82 (1.83)	2.03(5) (B)
${}^3B_2 \rightarrow ({}^3B_2 c)^k$	$(15b_2 \rightarrow 16b_2)$	2.33	2.04	2.03	—	—	—	—	—
${}^3B_2 \rightarrow ({}^5A_2 b)^k$	$11b_1 \rightarrow 23a_1$	(2.36)	(2.13)	(2.12)	—	—	—	—	—
${}^3B_2 \rightarrow ({}^3B_2 d)^k$	$(22a_1 \rightarrow 24a_1)$	2.76	2.27	2.27	—	—	—	—	—
${}^3B_2 \rightarrow {}^5B_2$	$21a_1 \rightarrow 23a_1$	(2.53)	(2.31)	(2.31)	2.20 (2.23)	2.06	2.35	2.36	2.3–2.8 (C)
${}^3B_2 \rightarrow {}^5A_1$	$14b_2 \rightarrow 23a_1$	(2.37)	(2.33)	(2.33)	2.40 (2.41)	1.92	2.32	2.33	—
${}^3B_2 \rightarrow {}^5B_1$	$5a_2 \rightarrow 23a_1$	(2.78)	—	—	2.75 (2.78)	2.43 (2.35)	2.81 (2.81)	2.82 (2.82)	3.25(5) (D)
$W_3O_8, {}^1A_1/C_{2v}$ (C)									
${}^1A_1 \rightarrow {}^3A_1$	$19a_1 \rightarrow 20a_1$	1.82 (2.53)	1.75 (2.31)	1.64 (2.31)	2.30 (2.92)	2.10	1.84	1.83	2.16(5) (A)
${}^1A_1 \rightarrow {}^3A_2$	$8a_2 \rightarrow 20a_1$	2.50 (2.66)	1.63 (1.75)	1.62 (1.75)	2.81 (2.89)	2.38 (2.39)	1.84 (1.86)	1.83 (1.84)	2.61(5) (B)
${}^1A_1 \rightarrow ({}^3B_1 a)$	$12b_1 \rightarrow 20a_1$	2.56 (2.70)	1.55 (1.66)	1.54 (1.66)	2.97 (3.27)	2.43 (2.44)	2.17	2.39	3.03(5) (C)
${}^1A_1 \rightarrow ({}^3B_1 b)^k$	$11b_1 \rightarrow 20a_1$	2.58 (2.74)	1.71 (1.82)	1.70 (1.82)	—	—	—	—	—
${}^1A_1 \rightarrow ({}^3B_2 b)$	$14b_2 \rightarrow 20a_1$	2.95 (3.24)	2.17 (2.38)	2.15 (2.38)	3.26 (3.40)	2.85 (2.93)	2.24 (2.28)	2.22 (2.27)	—
${}^1A_1 \rightarrow ({}^3A_2 b)^k$	$7a_2 \rightarrow 20a_1$	3.03 (3.20)	2.21 (2.33)	2.20 (2.33)	—	—	—	—	—
${}^1A_1 \rightarrow ({}^3A_1 b)^k$	$18a_1 \rightarrow 20a_1$	3.14 (3.53)	2.42 (2.79)	2.39 (2.79)	—	—	—	—	—
${}^1A_1 \rightarrow ({}^3B_2 c)^k$	$13b_2 \rightarrow 20a_1$	3.22 (3.66)	2.64 (2.86)	2.60 (2.85)	—	—	—	—	—
${}^1A_1 \rightarrow ({}^3B_1 c)^k$	$10b_1 \rightarrow 20a_1$	3.43 (3.66)	2.67 (2.83)	2.65 (2.82)	—	—	—	—	—

^a Defined as the difference between the vertical electron detachment energies to the excited and ground states of the neutral. ^b The corresponding electron excitation in the neutral. Those in parentheses are excitations to the unoccupied orbitals other than the LUMO. The electron configuration at the BP86/aVDZ level for the 3B_2 state of structure **A** of $Cr_3O_8^-$ at the geometry of the ground state of the anion is ... $(5a_2)^2(10b_1)^2(14b_2)^2(21a_1)^2(11b_1)^2(12b_1)^2(15b_2)^1(22a_1)^1(23a_1)^0(6a_2)^0(13b_1)^0(7a_2)^0(16b_2)^0(24a_1)^0$. The electron configuration at the B3LYP/aVDZ level for the 1A_1 state of structure **C** of $W_3O_8^-$ at the geometry of the ground state of the anion is ... $(10b_1)^2(13b_2)^2(18a_1)^2(7a_2)^2(14b_2)^2(19a_1)^2(11b_1)^2(8a_2)^2(12b_1)^2(20a_1)^0$. ^c Numbers in the parentheses are for the corresponding low spin states (triplets for $M = Cr$ and open-shell singlets for $M = W$). See text. ^d B3LYP/aVDZ. ^e BP86/aVDZ. ^f PW91/aVDZ. ^g CCSD(T)/aVDZ//B3LYP/aVDZ. ^h B3LYP/aVTZ//B3LYP/aVDZ. ⁱ BP86/aVTZ//BP86/aVDZ. ^j PW91/aVTZ//PW91/aVDZ. ^k This state is not the lowest energy state in this spin and spatial symmetry, and excitation energies are calculated at the TD-DFT level only.

D was calculated to be ~13 kcal/mol higher in energy than the 4B_2 state of structure **A** at the CCSD(T) and B3LYP levels with the aVTZ basis set (Table 2). We note that the BP86 and PW91 functionals predict that the 4A_2 state of structure **D** is the ground state. The calculated VDEs and ADEs with the BP86 and PW91 functionals for the 4A_2 state of structure **D** do not allow us at this level to distinguish between this state and the 4B_2 state (structure **A**). Based on the above comparison, the X band in the PES of $Cr_3O_8^-$ is best assigned to the ${}^4B_2 \rightarrow {}^3B_2$ transition of structure **A** at the CCSD(T) level but the BP86 and PW91 functionals do not allow us to completely eliminate the 4A_2 state of structure **D**. Other calculations on $(CrO_3)_n$ clusters show that the chain structures are usually much higher in energy, so it is unlikely to be present. In any case, a high spin ground state is predicted.

5.2. The X Band of $W_3O_8^-$. The ground state of $W_3O_8^-$ (the 2A_1 state of structure **C**) has an electron configuration of ... $(14b_2)^2(11b_1)^2(12b_1)^2(8a_2)^2(19a_1)^2(20a_1)^1$ at the B3LYP/aVDZ level (Figure 9). Removal of an electron from its SOMO leads to the 1A_1 state of the neutral. The ADE and VDE for the ${}^2A_1 \rightarrow {}^1A_1$ transition of structure **C** were calculated to be 3.86 and 4.45 eV at the CCSD(T)/aVTZ level (Table 5), which can be compared with the respective experimental values for the X band of 4.37 and 4.62 eV. The ADE and VDE are underestimated

by ~0.5 and 0.2 eV, respectively, consistent with the errors predicted for $W_3O_9^-$.³² We note that the VDE value is in quite good agreement, whereas the difficulty in extrapolating to the ADE contributes to the difference between theory and experiment. The ADE calculated at the CCSD(T)/aVTZ level is essentially the same as that calculated at the CCSD(T)/aVTZ level, and the VDE calculated at the CCSD(T)/aVDZ level is smaller by ~0.1 eV. The core-valence correction is ~0.1 eV. These results are also consistent with our recent benchmark study on the electron detachment energies of the MO_3^- and $M_2O_6^-$ ($M = Cr, Mo, W$) clusters for $M = W$.²⁴ Even though the ${}^2A'$ state of structure **B** is only 1–2 kcal/mol above the anion ground state (Table 3), the ADE and VDE calculated at the CCSD(T)/aVTZ level for the ${}^2A' \rightarrow {}^1A'$ transition are lower than the experimental values by 0.8–1.0 eV. The ${}^2A''$ state of structure **B** was predicted to be 4–5 kcal/mol higher in energy than the anion ground state, and the ADE and VDE calculated for the ${}^2A'' \rightarrow {}^1A'$ transition of structure **B** are also lower than the experimental values by 0.9–1.2 eV. Based on these comparisons, we can eliminate these states from contributing to the observed spectra.

5.3. Higher Binding Energy Bands. Table 6 lists calculated ADEs and VDEs to the excited states of the neutral from the anion ground state ($Cr_3O_8^-$, 4B_2 (**A**) and $W_3O_8^-$, 2A_1 (**C**)), which

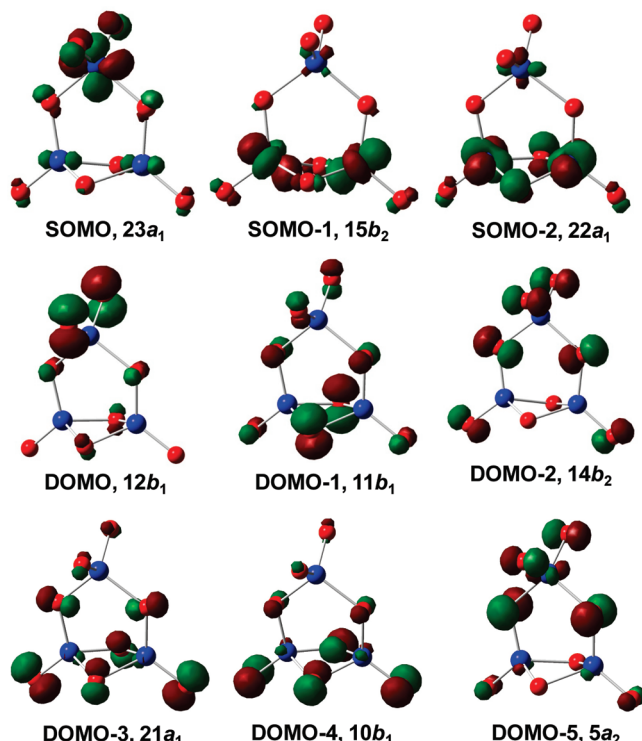


Figure 8. Singly occupied and highest few doubly occupied molecular orbitals (SOMOs and DOMOs) for the ground state of $Cr_3O_8^-$ at the BP86/aVDZ level.

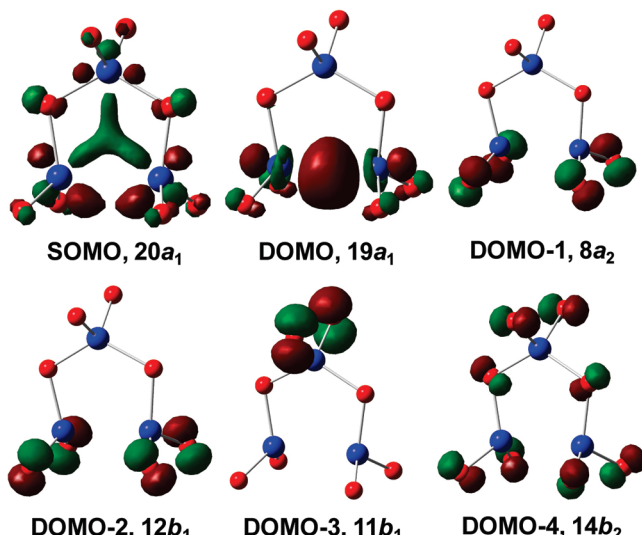


Figure 9. Singly occupied and highest few doubly occupied molecular orbitals (SOMOs and DOMOs) for the ground state of $W_3O_8^-$ at the B3LYP/aVDZ level.

are compared to the experimental values in order to assign the higher binding energy band systems in the PES. Additional calculated ADEs and VDEs for transitions that cannot be described as one electron processes are given as Supporting Information.

5.3.1. $Cr_3O_8^-$. Removal of an electron from the SOMOs $23a_1$, $15b_2$, and $22a_1$ of $Cr_3O_8^-$ (the 4B_2 state of structure **A**) leads to the 3B_2 ground state and the 3A_1 and $(^3B_2 b)$ excited states of the neutral, respectively. The 3A_1 excited state can be assigned to band A in the PES based on the calculated ADE and VDE at the CCSD(T)/aVTZ level (calculated, 4.85 and 5.26 eV; experimental, 4.78 and 4.95 eV in Table 6). The slight overestimation of the ADE and VDE is consistent with that for

the ground state transition (Table 4). As the $(^3B_2 b)$ excited state has the same spin and spatial symmetry as the 3B_2 ground state, it cannot be calculated with such ground state methods as CCSD(T) and DFT. At the TD-DFT level, however, the $(^3B_2 b)$ excited state was predicted to lie very close in energy to the 3A_1 excited state (Tables 8 and 9); thus, the $(^3B_2 b)$ excited state may also contribute to the A band.

Removal of an electron from the doubly occupied molecular orbitals (DOMOs) $12b_1$, $14b_2$, $21a_1$, and $5a_2$ leads to the quintet excited states 5A_2 , 5A_1 , 5B_2 , and 5B_1 and their corresponding triplet excited states. These quintet states are formed by removing an electron with β -spin, whereas these triplet states are formed by removing an electron with α -spin leaving a single β -spin electron in the orbital. Molecular structures of the quintet states are given as Supporting Information (Figure S2). The quintet and triplet states are expected to have similar energies in most cases as long as there is some spatial difference in the orbitals as the only difference is spin pairing of electrons in two open-shell orbitals. Relative energies between the quintet states and their corresponding triplet states are calculated at the neutral and anionic geometries (Table 7). The quintet state is calculated at the ROHF/aVDZ level, whereas the triplet state is calculated at the complete active space self-consistent field (CASSCF) level with the same basis set by occupying each of the four open-shell orbitals in the quintet state with exactly one electron. The triplet states are calculated to be slightly higher in energy than the quintet states by 0.3–0.7 kcal/mol at both geometries as expected.

The 5A_2 excited state can be assigned to band B in the PES based on the calculated ADE and VDE at the CCSD(T) level (calculated, 6.28 and 6.73 eV; experimental, 6.30 and 6.47 eV in Table 6). By comparing the VDEs calculated at the CCSD(T) level for these quintet states and the experimental VDEs for the C and D bands, the C band can be assigned to the $^4B_2 \rightarrow ^5A_1$ and $^4B_2 \rightarrow ^5B_2$ transitions (calculated, 7.24 and 7.04 eV; experimental, 6.7–7.2 eV), and the D band can be assigned to the $^4B_2 \rightarrow ^5B_1$ transition (calculated, 7.56 eV; experimental, 7.69 eV). The calculated VDEs to the corresponding triplet states are very close to those to the quintet states (Table 6), indicating these triplet states are likely to be contributing to bands B–D as well.

The VDEs calculated at the CCSD(T)/aVDZ level for the transitions from the 4B_2 state to the $(^3A_2 a)$, $(^3B_1 a)$, $(^3A_2 b)$, and $(^3B_1 b)$ states (Table S5, Supporting Information), which cannot be described as one-electron processes, are 0.8–1.3 eV higher than that of the A band, but are 0.2–0.5 eV lower than that of the B band. After geometry relaxation, all of these triplet states have one or more imaginary frequencies at the B3LYP/aVDZ, BP86/aVDZ, and PW91/aVDZ levels, so they will form lower symmetry structures; however, this does not affect the predicted VDEs. These shake-up transitions may contribute to the electron signals between band A and band B, consistent with their low intensities (Figure 1).

5.3.2. $W_3O_8^-$. For $W_3O_8^-$ (the 2A_1 state of structure **C**), removal of an electron from the DOMOs $19a_1$, $8a_2$, $12b_1$, and $14b_2$ leads to the triplet excited states 3A_1 , 3A_2 , $(^3B_1 a)$, and $(^3B_2 b)$, and the corresponding open-shell singlet states. Relative energies between the triplet states and their corresponding open-shell singlet states are calculated at the neutral and anionic geometries (Table 7). The triplet state is calculated at the ROHF/aVDZ level, whereas the open-shell singlet state is calculated at the CASSCF/aVDZ level by occupying each of the two open-shell orbitals in the triplet state with exactly one electron. The singlet states are calculated to be higher in energy than the triplet

TABLE 9: Lowest Few Excitation Energies in eV of M_3O_8 ($M = Cr, W$) Calculated at the TD-DFT Level with the B3LYP/aVDZ, BP86/aVDZ, and PW91/aVDZ Methods, Compared with the Adiabatic and Vertical Excitation Energies (AEEs and VEEs) Calculated Self-Consistently at the CCSD(T)/aVDZ//B3LYP/aVDZ, B3LYP/aVTZ//B3LYP/aVDZ, BP86/aVTZ//BP86/aVDZ, and PW91/aVTZ//PW91/aVDZ Levels

excitation	orbital ^a	TD-DFT			AEE				VEE			
		B3LYP ^b	BP86 ^c	PW91 ^d	CCSD(T) ^e	B3LYP ^f	BP86 ^g	PW91 ^h	CCSD(T) ^e	B3LYP ^f	BP86 ^g	PW91 ^h
$Cr_3O_8, {}^3B_2/C_{2v} (\mathbf{A})$												
${}^3B_2 \rightarrow ({}^3B_1 \mathbf{a})$	$22a_1 \rightarrow 6a_2$	0.96	0.78	0.76	0.89	1.16	0.65	0.64	0.99	1.30	0.75	0.74
${}^3B_2 \rightarrow ({}^3A_2 \mathbf{a})$	$15b_2 \rightarrow 6a_2$	1.06	0.98	0.96	0.71	1.20	0.49	0.49	1.25	1.76	0.98	0.98
${}^3B_2 \rightarrow ({}^3B_2 \mathbf{b})^i$	$22a_1 \rightarrow 23a_1$	2.17	1.07	1.07	—	—	—	—	—	—	—	—
${}^3B_2 \rightarrow {}^3A_1$	$15b_2 \rightarrow 23a_1$	2.37	1.17	1.18	0.55	1.00	0.62	0.63	1.98	2.31	1.46	1.48
${}^3B_2 \rightarrow ({}^3A_2 \mathbf{b})$	$22a_1 \rightarrow 13b_1$	2.86	1.42	1.40	1.15	1.58	0.99	0.99	1.34	1.81	1.20	1.20
${}^3B_2 \rightarrow ({}^3B_1 \mathbf{b})$	$15b_2 \rightarrow 13b_1$	2.60	1.57	1.55	1.26	1.80	1.13	1.12	1.58	2.13	1.41	1.41
${}^3B_2 \rightarrow ({}^3B_1 \mathbf{c})^i$	$22a_1 \rightarrow 7a_2$	2.82	1.95	1.94	—	—	—	—	—	—	—	—
${}^3B_2 \rightarrow ({}^3A_2 \mathbf{c})^i$	$15b_2 \rightarrow 7a_2$	2.62	2.15	2.15	—	—	—	—	—	—	—	—
${}^3B_2 \rightarrow {}^5A_2$	$12b_1 \rightarrow 23a_1$	(2.53) ^j	(2.27) ^j	(2.25) ^j	1.98	1.60	1.97	1.98	—	1.96	2.24	2.26
$Cr_3O_8, {}^3A''/C_s (\mathbf{B})$												
${}^3A'' \rightarrow {}^3A'$	$23a'' \rightarrow 32a'$	1.38	1.27	1.27	1.02	0.81	0.70	0.71	1.39	1.17	1.10	1.11
${}^3A'' \rightarrow ({}^3A'' \mathbf{b})^i$	$23a'' \rightarrow 24a''$	2.05	1.40	1.42	—	—	—	—	—	—	—	—
${}^3A'' \rightarrow ({}^3A'' \mathbf{c})^i$	$31a' \rightarrow 32a'$	1.49	1.54	1.53	—	—	—	—	—	—	—	—
${}^3A'' \rightarrow ({}^3A' \mathbf{b})$	$31a' \rightarrow 24a''$	2.51	1.65	1.67	1.72	1.67	1.34	1.33	—	2.40	1.88	1.90
$Cr_3O_8, {}^3B_2/D_{2d} (\mathbf{D})$												
${}^3B_2 \rightarrow {}^3A_2$	$12a_1 \rightarrow 3b_1$	0.51	0.59	0.55	0.42	0.37	0.36	0.34	0.41	0.38	0.47	0.45
${}^3B_2 \rightarrow {}^3B_1$	$12b_2 \rightarrow 3b_1$	0.35	0.80	0.78	0.29	0.15	0.59	—	0.29	0.16	—	—
${}^3B_2 \rightarrow ({}^3B_2 \mathbf{b})^i$	$12a_1 \rightarrow 13a_1$	2.43	1.14	1.12	—	—	—	—	—	—	—	—
${}^3B_2 \rightarrow {}^3A_1^i$	$12b_2 \rightarrow 13a_1$	2.46	1.61	1.60	—	—	—	—	—	—	—	—
$W_3O_8, {}^1A'/C_s (\mathbf{B})$												
${}^1A'/C_s \rightarrow {}^3A_2/C_{2v}$	$31a' \rightarrow 23a''$	1.00	1.56	1.48	0.42	0.24	0.56	0.57	1.23	1.11	1.52	1.54
${}^1A' \rightarrow {}^3A'$	$31a' \rightarrow 32a'$	1.57	1.70	1.56	1.55	1.37	1.28	1.28	1.89	1.68	1.67	1.68
$W_3O_8, {}^1A_1/C_{2v} (\mathbf{A})$												
${}^1A_1 \rightarrow {}^3A_2$	$22a_1 \rightarrow 6a_2$	1.44	1.45	1.44	0.79	0.60	0.57	0.60	1.66	1.48	1.44	1.47
${}^1A_1 \rightarrow {}^3A_1$	$22a_1 \rightarrow 23a_1$	1.81	1.56	1.55	1.03	0.88	0.76	0.77	2.13	1.88	1.68	1.72
${}^1A_1 \rightarrow {}^3B_2$	$22a_1 \rightarrow 15b_2$	2.11	2.54	2.49	0.24	-0.07	0.27	0.30	2.60	2.36	2.61	2.66
$W_3O_8, {}^1A_1/C_{2v} (\mathbf{C})$												
${}^1A_1 \rightarrow {}^3A_1$	$19a_1 \rightarrow 20a_1$	2.62	2.60	2.50	2.64	2.49	2.11	2.14	3.12	2.90	2.64	2.64
${}^1A_1 \rightarrow ({}^3B_2 \mathbf{a})$	$19a_1 \rightarrow 15b_2$	3.13	3.46	3.36	1.78	1.34	1.66	1.70	3.81	3.61	3.54	3.56
${}^1A_1 \rightarrow {}^3A_2$	$8a_2 \rightarrow 20a_1$	3.50	2.67	2.66	3.15	2.94	2.29	2.28	3.92	3.51	2.88	2.88
${}^1A_1 \rightarrow ({}^3B_1 \mathbf{a})$	$11b_1 \rightarrow 20a_1$	3.56	2.70	2.70	3.08	3.00	2.44	2.43	4.00	3.59	3.09	2.92
${}^1A_1 \rightarrow ({}^3B_1 \mathbf{d})$	$19a_1 \rightarrow 13b_1$	3.67	3.66	3.55	3.91	3.62	3.31	3.31	4.29	3.95	3.65	3.65
${}^1A_1 \rightarrow ({}^3B_1 \mathbf{b})^i$	$12b_1 \rightarrow 20a_1$	4.01	2.74	2.73	—	—	—	—	—	—	—	—
${}^1A_1 \rightarrow ({}^3B_2 \mathbf{b})$	$14b_2 \rightarrow 20a_1$	4.04	3.32	3.30	3.80	3.52	2.74	2.73	4.33	4.15	3.38	3.38

^a The corresponding electron excitation. The electron configuration at the BP86/aVDZ level for the 3B_2 state of structure **A** of Cr_3O_8 is $\dots(12b_1)^2(15b_2)^1(22a_1)^1(6a_2)^0(23a_1)^0(13b_1)^0(7a_2)^0$. That for the ${}^3A''$ state of structure **B** of Cr_3O_8 is $\dots(31a')^1(23a'')^1(32a')^0(24a'')^0$. That for the 3B_2 state of structure **D** of Cr_3O_8 is $\dots(12b_2)^1(12a_1)^1(3b_1)^0(13a_1)^0$. The electron configuration at the B3LYP/aVDZ level for the ${}^1A'$ state of structure **B** of W_3O_8 is $\dots(31a')^2(23a'')^0(32a')^0$. That for the 1A_1 state of structure **A** of W_3O_8 is $\dots(22a_1)^2(6a_2)^0(23a_1)^0(15b_2)^0$. That for the 1A_1 state of structure **C** of W_3O_8 is $\dots(14b_2)^2(11b_1)^2(12b_1)^2(8a_2)^2(19a_1)^2(20a_1)^0(15b_2)^0(13b_1)^0$. ^b B3LYP/aVDZ. ^c BP86/aVDZ. ^d PW91/aVDZ. ^e CCSD(T)/aVDZ//B3LYP/aVDZ. ^f B3LYP/aVTZ//B3LYP/aVDZ. ^g BP86/aVTZ//BP86/aVDZ. ^h PW91/aVTZ//PW91/aVDZ. ⁱ This state is not the lowest energy state in this spin and spatial symmetry, and excitation energies are calculated at the TD-DFT level only. ^j For the low spin triplet state 3A_2 .

states at both the anion and neutral geometries by 1.7–3.2 kcal/mol for the 3A_2 and ${}^3B_2 \mathbf{b}$ states, by 4.3–6.9 kcal/mol for the ${}^3B_1 \mathbf{a}$ state, and by 14–15 kcal/mol for the 3A_1 state. The large singlet–triplet splitting for the 3A_1 state is due to the fact that the open-shell orbitals $19a_1$ and $20a_1$ (the DOMO becomes singly occupied in the neutral; Figure 9) both have substantial electron density between the two bonded W atoms. The 3A_1 excited state can be assigned to band A in the PES based on the calculated ADE and VDE at the CCSD(T) level (calculated, 6.54 and 6.76 eV; experimental, 6.65 and 6.78 eV). By comparing the VDEs calculated at the CCSD(T) level and the experimental VDEs for the B and C bands, the B band can be assigned to the ${}^2A_1 \rightarrow {}^3A_2$ transition (calculated, 7.24 eV; experimental, 7.23 eV), and the C band can be assigned to the ${}^2A_1 \rightarrow ({}^3B_1 \mathbf{a})$ transitions (calculated, 7.40 eV; experimental, 7.65 eV). The ${}^2A_1 \rightarrow ({}^3B_2 \mathbf{b})$ transition may also contribute to band C (VDE calculated, 7.98 eV; experimental, 7.65 eV). The

calculated VDEs for the open-shell singlet states corresponding to the 3A_2 , ${}^3B_2 \mathbf{b}$, and ${}^3B_1 \mathbf{a}$ states are fairly close to these triplet states, indicating these singlet states are likely to contribute to bands A–C as well.

5.3.3. TD-DFT Excitation Energies. Our recent studies on chromium trioxide clusters have shown good agreement between the TD-DFT excitation energies at the anionic geometries and the calculated VDE differences from the anion to the ground and excited states of the neutral cluster.²⁰ Table 8 compares the excitation energies calculated at the TD-DFT level from the 3B_2 state of structure **A** for Cr_3O_8 and the 1A_1 state of structure **C** for W_3O_8 at the anion ground state geometries. They are compared to the experimental and calculated ΔE_{vert} values, which are defined as the differences between the VDEs to the ground and excited states of the neutral.

For Cr_3O_8 , the ΔE_{vert} values calculated at the CCSD(T)/aVDZ level for the 3A_1 , 5A_2 , 5A_1 , and 5B_2 states are in excellent

agreement with the experimental values for the A, B, and C bands within 0.1 eV, and that for the 5B_1 state is smaller than the experimental value for the D band by ~ 0.5 eV. The ΔE_{vert} values calculated at the CCSD(T)/aVDZ level for the ($^3B_1 \text{ } a$), ($^3A_2 \text{ } a$), ($^3A_2 \text{ } b$), ($^3B_1 \text{ } b$), and ($^3A_1 \text{ } b$) states are larger than that for the A band by ≥ 0.5 eV and smaller than that for the B band by more than 0.3 eV, consistent with the above spectral assignment. The ΔE_{vert} values were not calculated for several other states, as they are not the lowest energy state for their spin and spatial symmetry. The TD-DFT excitation energies for the 3A_1 and ($^3B_2 \text{ } b$) states calculated at the BP86/aVDZ and PW91/aVDZ levels are in good agreement with the experimental ΔE_{vert} value for the A band within 0.15 eV. Those for the 5A_2 and ($^5A_2 \text{ } b$) states (calculated from the TD-DFT triplet states corrected by the quintet-triplet splitting) are also within 0.15 eV of the experimental ΔE_{vert} value for the B band. The TD-DFT excitation energies for the 5B_2 and 5A_1 states (obtained by correcting the triplet states) also agree with the experimental ΔE_{vert} value for the C band. The TD-DFT excitation energies for the ($^3B_1 \text{ } a$), ($^3A_2 \text{ } a$), ($^3A_2 \text{ } b$), ($^3B_1 \text{ } b$), ($^3B_1 \text{ } c$), ($^3A_1 \text{ } b$), and ($^3A_2 \text{ } c$) states at the BP86/aVDZ and PW91/aVDZ levels range from 0.9 to 1.8 eV, which are larger than the experimental ΔE_{vert} value for the A band of 0.51 eV, but are smaller than that for the B band of 2.03 eV. The TD-DFT results for these triplet states are consistent with the CCSD(T) results, which show that transitions to these states are not one-electron transitions. The TD-DFT excitation energies for the ($^3B_2 \text{ } c$) and ($^3B_2 \text{ } d$) states are in good agreement with the experimental ΔE_{vert} values for bands B and C, respectively. Where a direct comparison can be made, the TD-DFT excitation energies calculated at the BP86/aVDZ and PW91/aVDZ levels for Cr_3O_8 at the anion ground state geometry are within ~ 0.1 eV from the ΔE_{vert} values calculated at the CCSD(T)/aVDZ level.

For W_3O_8 , the ΔE_{vert} values calculated at the CCSD(T)/aVDZ level for the 3A_1 , 3A_2 , and ($^3B_1 \text{ } a$) states are in good agreement with the experimental values for the A, B, and C bands within 0.2 eV. The TD-DFT excitation energy for the 3A_2 state calculated at the B3LYP/aVDZ level is in good agreement with the experimental ΔE_{vert} value for the B band within 0.15 eV, whereas those for the 3A_1 and ($^3B_1 \text{ } a$) states are lower than the experimental ΔE_{vert} values for the A and C bands by ~ 0.3 and 0.5 eV, respectively. The TD-DFT excitation energy for the ($^3B_1 \text{ } b$) state calculated at the B3LYP/aVDZ level is essentially the same as that for the ($^3B_1 \text{ } a$) state, indicating transitions to both states are likely to contribute to band C. Where a direct comparison can be made, the TD-DFT excitation energies calculated at the B3LYP/aVDZ level for W_3O_8 at the anion ground state geometry are lower than the ΔE_{vert} values calculated at the CCSD(T)/aVDZ level by 0.3–0.5 eV.

5.4. Comparison of $Cr_3O_8^-$ and $W_3O_8^-$. The $Cr_3O_8^-$ anion exhibits congested PES bands at lower binding energies (Figure 1), in contrast to $W_3O_8^-$ (Figure 2). The SOMOs and LUMO for the ground state of Cr_3O_8 (the 3B_2 state of structure **A**) consist of Cr 3d orbitals with minor contributions from the O 2p orbitals, which are similar to the SOMOs for the ground state of its anion (the 4B_2 state of structure **A**, Figure 8). Thus, the ground state and lowest few excited states for Cr_3O_8 arise mainly from Cr d–d transitions, which correspond to bands X and A with low binding energies and low excitation energies. The few highest energy DOMOs of the neutral and anion mainly consist of the O 2p π orbitals (Figure 8). The quintet excited states arising from these orbitals and the corresponding triplet states can be considered as O 2p π \rightarrow Cr 3d transitions, which have

significantly higher binding energies and correspond to bands B to D (Tables 6, 8, and 9).

Similar to the HOMO for the 1A_1 state of structure **C** of W_3O_8 , the highest DOMO for the anion ground state (the 2A_1 state of structure **C**, Figure 9) is primarily W–W σ bonding with predominant d character. The next few DOMOs are of O 2p π character mainly on the terminal oxygen atoms. The LUMO of the 1A_1 state of structure **C** of W_3O_8 is similar to the SOMO for the anion ground state (Figure 9), which is a d–d π orbital and the next few unoccupied MOs also consist of d orbitals on the W centers. The lowest two excited states for the 1A_1 state of structure **C** of W_3O_8 arise from the W–W bonding d orbitals and show high adiabatic excitation energies (AEE, 1.78 and 2.64 eV; Table 9), in contrast to those from the Cr–Cr nonbonding d orbital in Cr_3O_8 (AEE, 0.55 to 1.26 eV; Table 9). The lowest O 2p π \rightarrow W 5d excitation for W_3O_8 corresponds to band B (Tables 6 and 8).

6. Discussion

6.1. Cluster Structures and Metal–Metal Bonding. For both Cr_3O_8 and W_3O_8 clusters, multiple low-lying states were predicted within 15 kcal/mol at the CCSD(T)/aVDZ level: six states for Cr_3O_8 and five states for W_3O_8 (Figures 4 and 6). This is in contrast to the $(MO_3)_n$ ($M = Cr, Mo, W; n = 1–6$) clusters,²³ where no very-low-lying structures were predicted, except for $M = Mo$ and W for $n = 6$ due to substantial geometry changes. The situation of M_3O_8 is, however, similar to that for the $(TiO_2)_n$ ($n = 1–4$) clusters.²⁹ For these clusters, there are three very-low-lying structures for $n = 2–4$ within ~ 15 kcal/mol at the CCSD(T)/aVTZ level, likely due to the low oxygen–metal atom ratios, which enables the formation of more compact structures in order to increase the average number of oxygen atoms around each metal center.

Comparison of the relative energetics for the different structures for Cr_3O_8 and W_3O_8 shows that Cr_3O_8 prefers a high spin configuration whereas W_3O_8 prefers a low spin configuration. For structures **A** and **B**, the lowest triplet states of Cr_3O_8 are lower in energy than the lowest singlet states by ~ 7 and 19 kcal/mol, respectively, at the CCSD(T)/aVDZ level. For W_3O_8 , the lowest triplet states are higher in energy by ~ 6 and 10 kcal/mol, respectively. For structures **C** and **D**, both M_3O_8 clusters prefer the same spin multiplicity: the singlet state for structure **C** (due to potential metal–metal bonding) and the triplet state for structure **D**. However, the energy difference between the lowest singlet and triplet electronic states are very different for both structures. For structure **C**, the lowest triplet state is only ~ 7 kcal/mol higher in energy than the lowest singlet state for Cr_3O_8 , whereas the triplet is ~ 41 kcal/mol higher in energy than the singlet for W_3O_8 . For structure **D**, the lowest triplet state is ~ 14 kcal/mol lower than the lowest singlet state for Cr_3O_8 , whereas the triplet is only ~ 6 kcal/mol lower in energy than the singlet for W_3O_8 . The preference for high spin multiplicity for the chromium oxide cluster may be due to the larger repulsion between the 3d electrons as they are much closer to the nucleus than the 5d electrons in W. Similar conclusions can be reached for $Cr_3O_8^-$ and $W_3O_8^-$, as the ground state of $Cr_3O_8^-$ was predicted to be the 4B_2 state of structure **A**, and that of $W_3O_8^-$ was predicted to be the 2A_1 state of structure **C**. In fact, most of the low-lying states for $Cr_3O_8^-$ were predicted to be quartets, whereas all the low-lying states for $W_3O_8^-$ were predicted to be doublets. The electron spin densities for the open-shell ground state structures of Cr_3O_8 , $Cr_3O_8^-$, and $W_3O_8^-$ are depicted in Figure 10. The difference in the electron spin density for the ground states of Cr_3O_8 and $Cr_3O_8^-$ is that the two

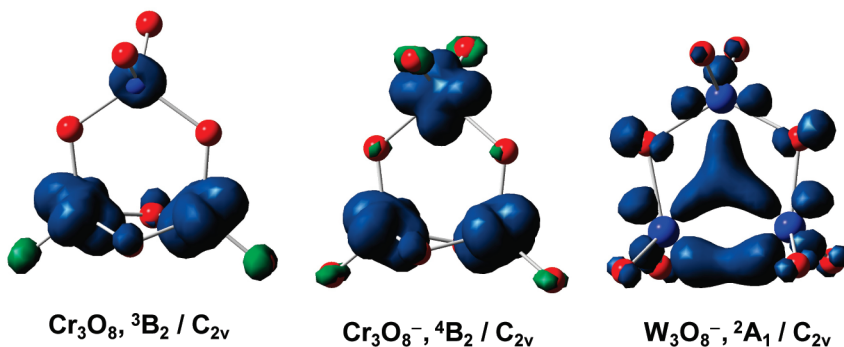


Figure 10. Electron spin density for the ground states of Cr_3O_8 , Cr_3O_8^- , and W_3O_8^- .

unpaired electrons in Cr_3O_8 are essentially localized on the two equivalent Cr centers, whereas in Cr_3O_8^- the three unpaired electrons are approximately equally distributed among the three Cr centers.

The HOMO for the ${}^1\text{A}_1$ (${}^1\text{A}$) state of structure **C** for W_3O_8 (Cr_3O_8) indicates the presence of metal–metal d–d σ bonding character. For Cr_3O_8 , this state is predicted to be ~ 38 kcal/mol higher in energy than its ground state, whereas for W_3O_8 it is predicted to be only ~ 8 kcal/mol above the ground state at the CCSD(T)/aVDZ level. The ground state of W_3O_8^- was predicted to be the ${}^2\text{A}_1$ state of this structure, and the anion clearly shows the presence of multicenter metal–metal d–d bonding (Figure 9). For Cr_3O_8^- , this state was predicted to be ~ 32 kcal/mol higher in energy than the ground state. The SOMO for the ground state of W_3O_8^- is similar to that for the ${}^2\text{A}_1'$ state of M_3O_9^- ($\text{M} = \text{Mo}$ and W) and the HOMO for the ${}^1\text{A}_1'$ state of $\text{M}_3\text{O}_9^{2-}$,^{26,32} in that they both display multicenter metal–metal d bonding character. The multicenter metal–metal d bonding is further enhanced by adding an extra electron to the SOMO of the ground state of W_3O_8^- to form the ${}^1\text{A}_1$ state of $\text{W}_3\text{O}_8^{2-}$, which is predicted to be 0.9 kcal/mol lower in energy than W_3O_8^- at the CCSD(T)/aVTZ level. By including the core–valence correction calculated at the CCSD(T)/awCVDZ level, the ${}^1\text{A}_1$ state of $\text{W}_3\text{O}_8^{2-}$ is predicted to be 2.5 kcal/mol lower in energy than the ground state of W_3O_8^- . The W–W bond length shrinks from the neutral (~ 2.90 Å), to the monoanion (~ 2.81 Å), to the dianion (~ 2.72 Å). Our prediction of the relative stability of the monoanion and dianion of W_3O_8 is consistent with that for W_3O_9 , where the ground state of $\text{W}_3\text{O}_9^{2-}$ was predicted to be 5.5 kcal/mol lower in energy than that of W_3O_9^- .³²

One can estimate the metal–metal bond energy in the ${}^1\text{A}_1$ state of structure **C** for M_3O_8 from the energy difference between this state and the ${}^3\text{B}_2$ state of the same structure, as the metal–metal bond is broken in this triplet state. The metal–metal bond energy estimated with this approach can be considered as a lower limit. For W_3O_8 , the W–W bond energy is estimated to be 41 kcal/mol at the CCSD(T)/aVDZ level. For Cr_3O_8 , the Cr–Cr bond energy is estimated to be only 7 kcal/mol. The calculated W–W bond lengths in both the ${}^1\text{A}_1$ and ${}^2\text{A}_1$ states of structure **C** are significantly longer than the WW multiple bond (2.1–2.3 Å)⁵¹ and double bond lengths (2.4–2.5 Å)^{52,53} but comparable to the typical WW single bonds (2.8–2.9 Å).^{52,54} This is consistent with the qualitative oxidation states of the W centers as there is one electron left over for each after accounting for the two terminal W=O bonds and the bridge W–O bond. The W–W single bond is likely to be very active and can be easily oxidized due to the much weaker metal–metal bond as compared to the very strong metal–oxygen bonds.²⁴

6.2. Performance of DFT. The current comparative study allows the evaluation of the performance of different DFT

exchange-correlation functionals for Cr versus W oxides. Due to the structural variety and d–d interaction (ferromagnetic versus antiferromagnetic spin coupling), the current reduced M_3O_8 and M_3O_8^- ($\text{M} = \text{Cr}, \text{W}$) clusters are more challenging than the stoichiometric $(\text{MO}_3)_n$ and $(\text{MO}_3)_n^-$ clusters.^{24,32} We expect the conclusions drawn here to be widely applicable to other Cr versus W compounds as well.

6.2.1. Relative Energies. The relative energies calculated at the B3LYP/aVTZ level in comparison with our best CCSD(T) values for W_3O_8 and its anion can have differences of up to 7 kcal/mol (Table 3). For Cr_3O_8 and its anion, the differences are up to 25 kcal/mol (Table S1, Supporting Information). For the ${}^2\text{A}'$ state of structure **B**, the difference is ~ 50 kcal/mol (Table 2), although in this case the CCSD(T) result is no longer accurate due to the significant multireference character of the wave function. The relative energies calculated at the BP86/aVTZ and PW91/aVTZ levels are very close to each other (Tables 2 and 3). They are within 3 kcal/mol of the CCSD(T) relative energies for W_3O_8 and its anion. For Cr_3O_8 and its anion, the differences are up to 8 kcal/mol, and for the ${}^4\text{A}_2$ state of structure **D** (Table 2) and the ${}^2\text{A}'$ state of structure **B** (Table S1, Supporting Information), the differences are ~ 15 and 25 kcal/mol, respectively. Thus, the relative energies calculated with the BP86 or PW91 functionals are usually closer to the CCSD(T) values than those with the B3LYP functional especially for systems with substantial multireference character, such as Cr, although they can give qualitatively different results from CCSD(T). Thus, DFT calculations for these challenging species should be carried out with at least two functionals, preferably one hybrid and one pure functional.

6.2.2. Electron Detachment Energies. For Cr_3O_8^- , the VDEs calculated at the B3LYP/aVTZ level are higher than the experimental value by 0.7–1.1 eV for bands X and A (Tables 4 and 6), but they are in good agreement with the experimental values for bands B–D (Table 6). For W_3O_8^- , the calculated VDEs are in good agreement with experiment within 0.2 eV for bands X–C (Tables 5 and 6). The VDEs calculated with the BP86 and PW91 functionals are close to each other as expected. For Cr_3O_8^- , they are in good agreement with the experimental value for band A, lower than the experimental values by 0.2–0.3 eV for bands X and C, and lower by 0.4–0.7 eV for bands B and D (Tables 4 and 6). For W_3O_8^- , the BP86 and PW91 values are in good agreement with the experimental value for band X, but lower than the experimental values by 0.3–0.8 eV for bands A–C (Tables 5 and 6). The performance for the B3LYP, BP86, and PW91 functionals in calculating VDEs is consistent with our recent benchmark studies²⁴ in that the BP86 and PW91 functionals are on par with the B3LYP functional for systems with less multireference character, for example, for the Mo and W oxides, and they significantly outperform the B3LYP functional in case of the strong multi-

reference systems, for example, for the Cr oxides. The performance difference is mainly due to the presence of some component of Hartree–Fock exchange in the hybrid functionals.

6.2.3. Electronic Excitation Energies: Self-Consistent DFT.

The AEEs and vertical excitation energies (VEEs) calculated self-consistently at the DFT levels are compared with those at CCSD(T) in Table 9, and the ΔE_{vert} values are compared with CCSD(T) and experimental values in Table 8. At the CCSD(T)/aVDZ level the AEEs to the lowest excited states calculated for the ground state of Cr_3O_8 (the 3B_2 state of structure **A**), the $^3A''$ state of structure **B**, and the 3B_2 state of structure **D** range from 0.3 to 1.0 eV. Those for the ground state of W_3O_8 (the $^1A'$ state of structure **B**) and the 1A_1 state of structure **A** range from 0.2 to 0.4 eV, and both are much smaller than that for the 1A_1 state of structure **C** by 1.3–1.5 eV. The ground state of M_3O_8 ($M = Cr$ and W) has very-low-lying excited states with the first AEE starting from ~ 0.2 eV. Due to the very low excitation energies for the majority of these structures, the low-lying excited states may play an important role in reactions involving these clusters. Our recent studies on the $(TiO_2)_n$ ($n = 1$ –4) clusters have shown that different structures of these clusters can have very different first excitation energies, which may play a role in their applications in photocatalysis.²⁹

For Cr_3O_8 , the ΔE_{vert} values calculated self-consistently at the BP86/aVTZ and PW91/aVTZ levels are in good agreement with the CCSD(T) values within 0.1–0.3 eV, and are also in good agreement with the experimental values within 0.2 eV for bands A–C and are lower than the experimental value by ~ 0.4 eV for band D (Table 8). The ΔE_{vert} values calculated self-consistently with the B3LYP functional are overestimated by 0.3–0.5 eV when compared to the CCSD(T) values, and are in worse agreement with experiment: ~ 0.4 eV higher for band A, and 0.7–0.8 eV lower for bands B and D.

For W_3O_8 , the ΔE_{vert} values calculated self-consistently at the BP86/aVTZ and PW91/aVTZ levels are significantly lower than those at the CCSD(T) level by 0.5–1.0 eV, and are also lower than the experimental values by ~ 0.3 eV for band A and by 0.6–0.9 eV for bands B and C. Those calculated at the B3LYP/aVTZ level are in better agreement with CCSD(T) values, and are lower by < 0.2 eV for bands A and B and by ~ 0.6 eV for band C compared to experimental measurements. Thus, as for the calculated relative energies and electron detachment energies, the calculated electronic excitation energies are in general better for Cr_3O_8 with the BP86 and PW91 functionals and better for W_3O_8 with the B3LYP functional.

6.2.4. Electronic Excitation Energies: TD-DFT.

Table 9 presents the excitation energies from some of the low-lying states of the neutral cluster calculated at the TD-DFT level at their equilibrium geometries. They are compared with the AEEs and VEEs calculated self-consistently at the CCSD(T) and DFT levels. As the excited states calculated at the TD-DFT level with the B3LYP functional tend to have significant mixing between different orbital transitions especially for $M = Cr$, their orbital assignments are approximate. Those calculated with the BP86 and PW91 functionals usually have much less mixing. Furthermore, the order of the excitation energies for the different excited states calculated at the TD-DFT level with the B3LYP functional can be quite different from those calculated with the BP86 and PW91 functionals.

For structure **A** of Cr_3O_8 , the excitation energies calculated at the TD-DFT level with the BP86 and PW91 functionals are in good agreement with the VEEs calculated at the CCSD(T) levels within 0.3 eV except for the 3A_1 state of structure **A**, where it is underestimated by TD-DFT by ~ 0.8 eV (Table 9).

The excitation energies calculated at the TD-DFT level with the B3LYP functional are in good agreement with the VEEs calculated at the CCSD(T) level for the $(^3B_1 \mathbf{a})$, $(^3A_2 \mathbf{a})$, and 3A_1 states, but they are overestimated by 1.0–1.5 eV for the $(^3A_2 \mathbf{b})$ and $(^3B_1 \mathbf{b})$ states. The excitation energy to the $(^3B_2 \mathbf{b})$ state calculated at the TD-DFT level with the B3LYP functional is ~ 1.1 eV larger than those calculated with the BP86 and PW91 functionals.

The TD-DFT excitation energies calculated at the anion ground state geometries for the band A of Cr_3O_8 with the BP86 and PW91 functionals are in excellent agreement with the experimental ΔE_{vert} value, whereas that calculated with the B3LYP functional is higher by ~ 0.7 eV (Table 8). The TD-DFT excitation energies for the quintet states (by correcting the TD-DFT triplet state energies) at the B3LYP, BP86, and PW91 levels are in good agreement with the experimental values within 0.2 eV for bands B and C.

For structure **C** of W_3O_8 , the excitation energies calculated at the TD-DFT level with the B3LYP functional are smaller than the VEEs calculated at the CCSD(T) level by 0.3–0.7 eV (Table 9). Those calculated at the TD-DFT level with the BP86 and PW91 functionals are smaller than the VEEs calculated at the CCSD(T) level by up to 1.3 eV.

Compared to the experimental values, the TD-DFT excitation energies of W_3O_8 at the anion ground state geometries (Table 9) calculated with the BP86 and PW91 functionals are lower than experiment by 0.4–0.5 eV for band A, by ~ 1.0 eV for band B, and by ~ 1.5 eV for band C. Those calculated with the B3LYP functional are lower than the experimental values by < 0.3 eV for bands A and B, and by ~ 0.5 eV for band C. The above comparison between the excitation energies calculated self-consistently and those calculated at the TD-DFT level indicates the TD-DFT method is useful for locating low-lying excited states for these TMO clusters where there may be many closely lying electronic states, but there may be substantial error in the TD-DFT excitation energies.

6.3. Clustering Energies and Heats of Formation. We have recently developed an accurate approach to calculate the heats of formation of large TMO clusters from the heat of formation of the monomer and the normalized clustering energies (NCEs) of the large clusters, which has been successfully applied to group IVB and VIB TMO clusters up to the tetramers.^{29,55} We now apply this approach to the reduced TMO clusters M_3O_8 ($M = Cr, W$), with the clustering energy of M_3O_8 defined as

$$\Delta E(M_3O_8) = E(MO_2) + 2E(MO_3) - E(M_3O_8) \quad (1)$$

The heat of formation of M_3O_8 is then given as

$$\Delta H_{f,0K}(M_3O_8) = \Delta H_{f,0K}(MO_2) + 2\Delta H_{f,0K}(MO_3) - \Delta E(M_3O_8) \quad (2)$$

The results are presented in Table 10 with more details given as Supporting Information (Tables S6–S9). Following our previous work,⁵⁵ the total atomization energy (TAE) was calculated to be 229.4 kcal/mol for the ground state of CrO_2 ($^3B_1/C_{2v}$) and 318.7 kcal/mol for that of WO_2 ($^1A_1/C_{2v}$) at the CCSD(T)/CBS level including additional corrections (Supporting Information), giving $\Delta H_f(CrO_2) = -16.9$ and -17.3 kcal/mol, and $\Delta H_f(WO_2) = 2.3$ and 1.7 kcal/mol at 0 and 298 K, respectively. Our calculated heat of formation of CrO_2 is in excellent agreement with the JANAF value of -18.0 ± 10 kcal/mol at 298 K,⁵⁶ taken from the equilibrium vaporization of Cr_2O_3 .

TABLE 10: Clustering Energies at 0 K ($\Delta E_{0\text{K}}$), Heats of Formation at 0 and 298 K ($\Delta H_{f,0\text{K}}$ and $\Delta H_{f,298\text{K}}$), and Reaction Energies at 298 K ($\Delta H_{298\text{K}}$) in kcal/mol Calculated at the CCSD(T) Level^a

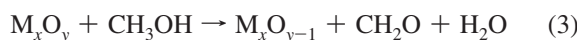
	M = Cr	M = W
clustering energy, $\Delta E_{0\text{K}}(\text{M}_3\text{O}_8)$	187.0	224.6
heat of formation		
$\Delta H_{f,0\text{K}}(\text{MO}_2)$	-16.9	-2.3
$\Delta H_{f,298\text{K}}(\text{MO}_2)$	-17.3	-1.7
$\Delta H_{f,0\text{K}}(\text{M}_3\text{O}_8)$	-326.7	-383.9
$\Delta H_{f,298\text{K}}(\text{M}_3\text{O}_8)$	-329.9	-386.8
reaction energy, $\Delta H_{298\text{K}}$		
$\text{M}_3\text{O}_9 + \text{CH}_3\text{OH} \rightarrow \text{M}_3\text{O}_8 + \text{CH}_2\text{O} + \text{H}_2\text{O}$	-9.0	+59.2
$\text{M}_3\text{O}_8 + (1/2)\text{O}_2 \rightarrow \text{M}_3\text{O}_9$	-26.9	-95.1

^a Error bars in the calculated heats of formation due to errors in the experimental heats of formation of the atoms are ± 1 kcal/mol for CrO_2 , ± 1.5 kcal/mol for WO_2 , ± 3 kcal/mol for Cr_3O_8 , and ± 4.5 kcal/mol for W_3O_8 . Theoretical heats of formation are taken from ref 55 for CrO_3 (-61.4 kcal/mol) and WO_3 (-78.5 kcal/mol) at 0 K, Cr_3O_9 (-356.8 kcal/mol) and W_3O_9 (-481.9 kcal/mol) at 298 K, and from ref 61 for CH_3OH (-48.0 \pm 0.6 kcal/mol), H_2O (-57.8 \pm 0.2 kcal/mol), and CH_2O (-26.1 \pm 0.3 kcal/mol) at 298 K.

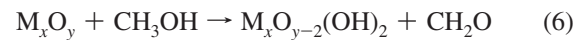
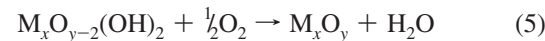
work of Grimley et al.⁵⁷ Our calculated heat of formation of WO_2 differs from the JANAF value of 18.3 ± 7 kcal/mol at 298 K based on the partial pressure work of DeMaria et al.⁵⁸ as well as the experimental value of 13.2 kcal/mol from the mass spectrometric study of Chupka et al.⁵⁹ The difference in the calculated heat of formation for WO_2 from experiment is similar to that for WO_3 ,⁵⁵ -79.6 kcal/mol calculated versus -70.0 \pm 7 kcal/mol from experiment at 298 K. As the calculated values are more negative than the experimental ones, we prefer our values.

The clustering energies for the ground states of Cr_3O_8 (the $^3\text{B}_2$ state of structure **A**) and W_3O_8 (the $^1\text{A}'$ state of structure **B**) as defined in eq 1 were calculated to be 187.0 and 224.6 kcal/mol at the CCSD(T)/aVTZ level with the core-valence correction calculated up to the CCSD(T)/wCVTZ level. The basis set dependence for the calculated clustering energy at the CCSD(T) level for M_3O_8 (Supporting Information) is similar to that for M_3O_9 ,⁵⁵ and we expect that the clustering energy in eq 1 for M_3O_8 calculated at the CCSD(T)/aVTZ level is essentially converged to the CBS limit. The heat of formation of M_3O_8 calculated from eq 2 with the heats of formation of MO_2 and MO_3 at the CCSD(T)/CBS level and the clustering energy of M_3O_8 at the CCSD(T)/aVTZ level is -326.7 and -329.9 kcal/mol for M = Cr, and -383.9 and -386.8 kcal/mol for M = W at 0 and 298 K, respectively. Our calculated heat of formation of W_3O_8 is to be compared with the JANAF value of -408.7 \pm 10 kcal/mol at 298 K based on the work of Ackermann and Rauh.⁶⁰

6.4. Redox Chemistry. Oxidative dehydrogenation (ODH) of CH_3OH can be used to probe the redox properties of TMO clusters. The catalytic process can be written as a two-stage global process. The first stage conceptually is the reduction of TMO clusters by CH_3OH to form CH_2O and H_2O (reaction 3), and the second stage is the subsequent oxidation of reduced TMO clusters by O_2 to regenerate the catalyst (reaction 4), with each stage involving multiple elementary steps.



Reaction enthalpies at 298 K for the above reactions for M_3O_9 can be obtained from our calculated heats of formation at 298 K for M_3O_9 (-356.8 and -481.9 kcal/mol for M = Cr and W, respectively)⁵⁵ and M_3O_8 , and those for CH_3OH (-48.0 kcal/mol), CH_2O (-26.1 kcal/mol), and H_2O (-57.8 kcal/mol) from Feller et al.⁶¹ As shown in Table 10, at 298 K reaction 3 is predicted to be exothermic for Cr_3O_9 by -9.0 kcal/mol, but endothermic for W_3O_9 by 59.2 kcal/mol. This is not surprising as Cr_3O_9 is a stronger oxidant than W_3O_9 and the $\text{W}=\text{O}$ bond energy (153 kcal/mol) is much larger than the $\text{Cr}=\text{O}$ bond energy (111 kcal/mol).⁵⁵ At 298 K, reaction 4 is predicted to be exothermic for both oxides, -26.9 kcal/mol for M = Cr and -95.1 kcal/mol for M = W, and the oxidation of W_3O_8 is much more exothermic than that for Cr_3O_8 . The high endothermicity for reaction 3 for W_3O_9 may prevent the complete oxidation of CH_3OH , enabling it to be used as a potential catalyst. The water elimination can occur in a reaction coupled to the exothermic oxidation step as shown in reaction 5, where the $\text{M}_x\text{O}_{y-2}(\text{OH})_2$ species is generated by reaction 6.



In reaction 5, dehydration is facilitated by the high exothermicity of the cluster oxidation.

7. Conclusions

In conclusion, we have conducted a comparative study of reduced transition metal oxide clusters, M_3O_8^- (M = Cr, W) anions and their neutrals, via anion photoelectron spectroscopy and density functional theory and molecular orbital theory (CCSD(T)) calculations. Well-resolved PES spectra are obtained for M_3O_8^- (M = Cr, W) at 193 and 157 nm detachment photon energies, and very different overall PES patterns are observed for the Cr versus W species. Extensive DFT and CCSD(T) calculations are performed to locate the ground and low-lying excited states for the neutrals and anions. The ground states of Cr_3O_8 and Cr_3O_8^- are predicted to be the $^3\text{B}_2$ and $^4\text{B}_2$ states of structure **A**, respectively, revealing ferromagnetic coupling in the species. In contrast, the ground states of W_3O_8 and W_3O_8^- are the $^1\text{A}'$ state of structure **B** and the $^2\text{A}_1$ state of structure **C**, respectively, showing strong metal–metal d–d bonding in the anion. The M_3O_8^- (M = Cr, W) cluster geometries are in qualitative agreement with prior DFT studies at the PBE level for M = Cr and at the B3LYP level for M = W. The current combined experimental and theoretical data also benchmark the performance of DFT methods for the Cr versus W oxide clusters.

Multiple low-lying excited states were located for reduced oxide clusters such as Cr_3O_8 and W_3O_8 , in contrast to the stoichiometric $(\text{MO}_3)_n$ (M = Cr, W) clusters. This may have significant catalytic implications. As the relative energies between the different structures depend strongly on the metal, the cluster size, and the chemical environment, very different chemistry may be accomplished by slight variations in the chemical composition of the catalyst. Thus, a thorough understanding of the relationship between the chemical structure and the catalytic reactivity and selectivity is critical for rational design of catalysts. The many possible low-lying structures also pose a significant challenge to the successful modeling of

catalytic processes involving redox chemistry using the metal oxide clusters as chemical models. For larger metal oxide clusters, even more low-lying structures may be expected, due to the increasing numbers of possible atomic arrangements. The chemical modeling of the catalytic processes is further complicated by the difficulty in predicting accurate relative energies with computationally efficient methods such as DFT. This needs to be addressed by more comprehensive benchmarking of these methods against highly accurate calculations and experimental measurements.

We applied our recently developed approach for calculating accurate heats of formation for TMO clusters from the normalized clustering energies to these reduced oxide clusters. The heats of formation of M_3O_8 are calculated from the generalized clustering energy of M_3O_8 and the calculated heats of formation for the monomers, MO_2 and MO_3 . We use the calculated heats of formation to predict the reaction energetics for the two global reactions in the oxidation dehydrogenation of CH_3OH catalyzed by M_3O_9 . The reduction step is predicted to be slightly exothermic for $M = Cr$. It is calculated to be very endothermic for $M = W$, which is likely to be important for preventing complete oxidation of the organic alcohol.

Acknowledgment. This work was supported by the Chemical Sciences, Geosciences and Biosciences Division, Office of Basic Energy Sciences, U.S. Department of Energy (DOE) under Grant DE-FG02-03ER15481 (catalysis center program) and was performed, in part, in the W. R. Wiley Environmental Molecular Sciences Laboratory including the Molecular Science Computing Facility, a national scientific user facility sponsored by DOE's Office of Biological and Environmental Research and located at the Pacific Northwest National Laboratory, operated for DOE by Battelle. D.A.D. also thanks the Robert Ramsay Chair Fund of The University of Alabama for support.

Supporting Information Available: Figures: Low-lying structures of M_3O_9 ($M = Cr, W$); additional electronic states for M_3O_8 and $M_3O_8^-$. Tables: additional relative energies for M_3O_8 and $M_3O_8^-$; additional ADEs and VDEs for $M_3O_8^-$; zero-point energies, electronic energies, core-valence corrections and T_1 diagnostics for M_3O_8 and $M_3O_8^-$; equilibrium geometries for M_3O_8 and $M_3O_8^-$. This material is available free of charge via the Internet at <http://pubs.acs.org>.

References and Notes

- (1) Rao, C. N. R.; Raveau, B. *Transition Metal Oxides*; Wiley-VCH: New York, 1998.
- (2) Weckhuysen, B. M.; Wachs, I. E.; Schoonheydt, R. A. *Chem. Rev.* **1996**, *96*, 3327.
- (3) (a) Schwarz, K. *J. Phys. F* **1986**, *16*, L211. (b) Kamper, K. P.; Schmitt, W.; Guntherodt, G.; Gambino, R. J.; Ruf, R. *Phys. Rev. Lett.* **1987**, *59*, 2788. (c) Korotin, M. A.; Anisimov, V. I.; Khomskii, D. I.; Sawatzky, G. A. *Phys. Rev. Lett.* **1998**, *80*, 4305.
- (4) For a recent review on gas-phase catalysis, see: Böhme, D. K.; Schwarz, H. *Angew. Chem., Int. Ed.* **2005**, *44*, 2336.
- (5) Ivanov, A. A.; Demidov, A. V.; Popenko, N. I.; Zasorin, E. Z.; Spiridonov, V. P. *J. Mol. Struct.* **1980**, *63*, 121.
- (6) Hop, C. E. C. A.; McMahon, T. B. *J. Am. Chem. Soc.* **1992**, *114*, 1237.
- (7) (a) Hachimi, A.; Poitevin, E.; Krier, G.; Muller, J. F.; Ruiz-Lopez, M. F. *Int. J. Mass Spectrom. Ion Process.* **1995**, *144*, 23. (b) Aubriet, F.; Maunut, B.; Muller, J. F. *Int. J. Mass Spectrom.* **2001**, *209*, 5. (c) Aubriet, F.; Muller, J. F. *J. Phys. Chem. A* **2002**, *106*, 6053.
- (8) Fiedler, A.; Kretzschmar, I.; Schroder, D.; Schwarz, H. *J. Am. Chem. Soc.* **1996**, *118*, 9941.
- (9) Chertihin, G. V.; Bare, W. D.; Andrews, L. *J. Chem. Phys.* **1997**, *107*, 2798.
- (10) (a) Wentholt, P. G.; Gunion, R. F.; Lineberger, W. C. *Chem. Phys. Lett.* **1996**, *258*, 101. (b) Wentholt, P. G.; Jonas, K. L.; Lineberger, W. C. *J. Chem. Phys.* **1997**, *106*, 9961.
- (11) Van Stipdonk, M. J.; Justes, D. R.; Schweikert, E. A. *Int. J. Mass Spectrom.* **2000**, *203*, 59.
- (12) (a) Wang, X.; Neukermans, S.; Vanhoutte, F.; Janssens, E.; Verschoren, G.; Silverans, R. E.; Lievens, P. *Appl. Phys. B: Laser Opt.* **2001**, *73*, 417. (b) Janssens, E.; Hou, X. J.; Neukermans, S.; Wang, X.; Silverans, R. E.; Lievens, P.; Nguyen, M. T. *J. Phys. Chem. A* **2007**, *111*, 4150.
- (13) (a) Gianotto, A. K.; Hodges, B. D. M.; Benson, M. T.; Harrington, P. de B.; Appelhans, A. D.; Olson, J. E.; Groenewold, G. S. *J. Phys. Chem. A* **2003**, *107*, 5948. (b) Gianotto, A. K.; Hodges, B. D. M.; Harrington, P. de B.; Appelhans, A. D.; Olson, J. E.; Groenewold, G. S. *J. Am. Soc. Mass Spectrom.* **2003**, *14*, 1067.
- (14) (a) Tono, K.; Terasaki, A.; Ohta, T.; Kondow, T. *Phys. Rev. Lett.* **2003**, *90*, 133402. (b) Tono, K.; Terasaki, A.; Ohta, T.; Kondow, T. *J. Chem. Phys.* **2003**, *119*, 11221.
- (15) Bergeron, D. E.; Castleman, A. W., Jr.; Jones, N. O.; Khanna, S. N. *Nano Lett.* **2004**, *4*, 261.
- (16) Molek, K. S.; Reed, Z. D.; Ricks, A. M.; Duncan, M. A. *J. Phys. Chem. A* **2007**, *111*, 8080.
- (17) Gutsev, G. L.; Jena, P.; Zhai, H. J.; Wang, L. S. *J. Chem. Phys.* **2001**, *115*, 7935.
- (18) Zhai, H. J.; Huang, X.; Waters, T.; Wang, X. B.; O'Hair, R. A. J.; Wedd, A. G.; Wang, L. S. *J. Phys. Chem. A* **2005**, *109*, 10512.
- (19) Zhai, H. J.; Wang, L. S. *J. Chem. Phys.* **2006**, *125*, 164315.
- (20) Zhai, H. J.; Li, S. G.; Dixon, D. A.; Wang, L. S. *J. Am. Chem. Soc.* **2008**, *130*, 5167.
- (21) (a) Reddy, B. V.; Khanna, S. N. *Phys. Rev. Lett.* **1999**, *83*, 3170. (b) Reddy, B. V.; Khanna, S. N.; Ashman, C. *Phys. Rev. B* **2000**, *61*, 5797.
- (22) (a) Veliyah, S.; Xiang, K. H.; Pandey, R.; Recio, J. M.; Newsam, J. M. *J. Phys. Chem. B* **1998**, *102*, 1126. (b) Xiang, K. H.; Pandey, R.; Recio, J. M.; Francisco, E.; Newsam, J. M. *J. Phys. Chem. A* **2000**, *104*, 990. (c) Lau, K. C.; Kandalam, A. K.; Costales, A.; Pandey, R. *Chem. Phys. Lett.* **2004**, *393*, 112.
- (23) Li, S. G.; Dixon, D. A. *J. Phys. Chem. A* **2006**, *110*, 6231.
- (24) Li, S. G.; Dixon, D. A. *J. Phys. Chem. A* **2007**, *111*, 11908.
- (25) Zhai, H. J.; Huang, X.; Cui, L. F.; Li, X.; Li, J.; Wang, L. S. *J. Phys. Chem. A* **2005**, *109*, 6019.
- (26) Huang, X.; Zhai, H. J.; Kiran, B.; Wang, L. S. *Angew. Chem., Int. Ed.* **2005**, *44*, 7251.
- (27) Huang, X.; Zhai, H. J.; Li, J.; Wang, L. S. *J. Phys. Chem. A* **2006**, *110*, 85.
- (28) (a) Zhai, H. J.; Kiran, B.; Cui, L. F.; Li, X.; Dixon, D. A.; Wang, L. S. *J. Am. Chem. Soc.* **2004**, *126*, 16134. (b) Huang, X.; Zhai, H. J.; Waters, T.; Li, J.; Wang, L. S. *Angew. Chem., Int. Ed.* **2006**, *45*, 657. (c) Zhai, H. J.; Wang, L. S. *J. Am. Chem. Soc.* **2007**, *129*, 3022. (d) Zhai, H. J.; Döbler, J.; Sauer, J.; Wang, L. S. *J. Am. Chem. Soc.* **2007**, *129*, 13270.
- (29) Li, S. G.; Dixon, D. A. *J. Phys. Chem. A* **2008**, *112*, 6646.
- (30) Zhai, H. J.; Averkiev, B. B.; Zubarev, D. Yu.; Wang, L. S.; Boldyrev, A. I. *Angew. Chem., Int. Ed.* **2007**, *46*, 4277.
- (31) Zubarev, D. Yu.; Averkiev, B. B.; Zhai, H. J.; Wang, L. S.; Boldyrev, A. I. *Phys. Chem. Chem. Phys.* **2008**, *10*, 257.
- (32) Li, S. G.; Dixon, D. A. *J. Phys. Chem. A* **2007**, *111*, 11093.
- (33) Dachsel, H.; Harrison, R. J.; Dixon, D. A. *J. Phys. Chem. A* **1999**, *103*, 152.
- (34) Sun, Q.; Rao, B. K.; Jena, P.; Stolcic, D.; Kim, Y. D.; Ganter, G.; Castleman, A. W., Jr. *J. Chem. Phys.* **2004**, *121*, 9417.
- (35) (a) Wang, L. S.; Cheng, H. S.; Fan, J. *J. Chem. Phys.* **1995**, *102*, 9480. (b) Wang, L. S.; Wu, H. In *Advances in Metal and Semiconductor Clusters*; Duncan, M. A., Ed.; JAI Press: Greenwich, CT, 1998; Vol. 4, Cluster Materials; pp 299–343.
- (36) (a) Wang, L. S.; Li, X. In *Clusters and Nanostructure Interfaces*; Jena, P.; Khanna, S. N.; Rao, B. K., Eds.; World Scientific: River Edge, NJ, 2000; pp 293–300. (b) Akola, J.; Manninen, M.; Hakkinen, H.; Landman, U.; Li, X.; Wang, L. S. *Phys. Rev. B* **1999**, *60*, R11297. (c) Wang, L. S.; Li, X.; Zhang, H. F. *Chem. Phys.* **2000**, *262*, 53. (d) Zhai, H. J.; Wang, L. S.; Alexandrova, A. N.; Boldyrev, A. I. *J. Chem. Phys.* **2002**, *117*, 7917.
- (37) (a) Becke, A. D. *J. Chem. Phys.* **1993**, *98*, 5648. (b) Lee, C.; Yang, W.; Parr, R. G. *Phys. Rev. B* **1988**, *37*, 785.
- (38) (a) Becke, A. D. *Phys. Rev. A* **1988**, *38*, 3098. (b) Perdew, J. P. *Phys. Rev. B* **1986**, *33*, 8822.
- (39) (a) Burke, K.; Perdew, J. P.; Wang, Y. In *Electronic Density Functional Theory: Recent Progress and New Directions*; Dobson, J. F., Vignale, G., Das, M. P., Eds.; Plenum: New York, 1998. (b) Perdew, J. P.; Wang, Y. *Phys. Rev. B* **1992**, *45*, 13244.
- (40) Kendall, R. A.; Dunning, T. H., Jr.; Harrison, R. J. *J. Chem. Phys.* **1992**, *96*, 6796.
- (41) (a) Peterson, K. A.; Figgen, D.; Dolg, M.; Stoll, H. *J. Chem. Phys.* **2007**, *126*, 124101. (b) Figgen, D.; Peterson, K. A.; Dolg, M.; Stoll, H. *J. Chem. Phys.* **2009**, *130*, 164108.
- (42) (a) Purvis, G. D., III; Bartlett, R. J. *J. Chem. Phys.* **1982**, *76*, 1910. (b) Raghavachari, K.; Trucks, G. W.; Pople, J. A.; Head-Gordon, M. *Chem. Phys.*

- Lett.* **1989**, *157*, 479. (c) Watts, J. D.; Gauss, J.; Bartlett, R. J. *J. Chem. Phys.* **1993**, *98*, 8718. (d) Bartlett, R. J.; Musial, M. *Rev. Mod. Phys.* **2007**, *79*, 291.
- (43) (a) Deegan, M. J. O.; Knowles, P. J. *Chem. Phys. Lett.* **1994**, *227*, 321. (b) Knowles, P. J.; Hampel, C.; Werner, H.-J. *J. Chem. Phys.* **1993**, *99*, 5219. (c) Rittby, M.; Bartlett, R. J. *J. Phys. Chem.* **1988**, *92*, 3033.
- (44) (a) Woon, D. E.; Dunning, T. H., Jr. *J. Chem. Phys.* **1995**, *103*, 4572. (b) Peterson, K. A.; Dunning, T. H., Jr. *J. Chem. Phys.* **2002**, *117*, 10548.
- (45) (a) Peterson, K. A.; Xantheas, S. S.; Dixon, D. A.; Dunning, T. H., Jr. *J. Phys. Chem. A* **1998**, *102*, 2449. (b) Feller, D.; Peterson, K. A. *J. Chem. Phys.* **1998**, *108*, 154. (c) Dixon, D. A.; Feller, D. *J. Phys. Chem. A* **1998**, *102*, 8209. (d) Feller, D.; Peterson, K. A. *J. Chem. Phys.* **1999**, *110*, 8384. (e) Feller, D.; Dixon, D. A. *J. Phys. Chem. A* **1999**, *103*, 6413. (f) Feller, D. *J. Chem. Phys.* **1999**, *111*, 4373. (g) Feller, D.; Dixon, D. A. *J. Phys. Chem. A* **2000**, *104*, 3048. (h) Feller, D.; Sordo, J. A. *J. Chem. Phys.* **2000**, *113*, 485. (i) Feller, D.; Dixon, D. A. *J. Chem. Phys.* **2001**, *115*, 3484. (j) Dixon, D. A.; Feller, D.; Sandrone, G. *J. Phys. Chem. A* **1999**, *103*, 4744. (k) Ruscic, B.; Wagner, A. F.; Harding, L. B.; Asher, R. L.; Feller, D.; Dixon, D. A.; Peterson, K. A.; Song, Y.; Qian, X.; Ng, C.; Liu, J.; Chen, W.; Schwenke, D. W. *J. Phys. Chem. A* **2002**, *106*, 2727. (l) Feller, D.; Dixon, D. A.; Peterson, K. A. *J. Phys. Chem. A* **1998**, *102*, 7053. (m) Dixon, D. A.; Feller, D.; Peterson, K. A. *J. Chem. Phys.* **2001**, *115*, 2576. (n) Dixon, D. A.; Gutowski, M. *J. Phys. Chem. A* **2005**, *109*, 5129. (o) Grant, D.; Dixon, D. A. *J. Phys. Chem. A* **2005**, *109*, 10138. (p) Matus, M. H.; Anderson, K. D.; Camaiioni, D. M.; Autrey, S. T.; Dixon, D. A. *J. Phys. Chem. A* **2007**, *111*, 4411. (q) Pollack, L.; Windus, T. L.; de Jong, W. A.; Dixon, D. A. *J. Phys. Chem. A* **2005**, *109*, 6934.
- (46) (a) Jamorski, C.; Casida, M. E.; Salahub, D. R. *J. Chem. Phys.* **1996**, *104*, 5134. (b) Bauernschmitt, R.; Ahlrichs, R. *Chem. Phys. Lett.* **1996**, *256*, 454. (c) Bauernschmitt, R.; Häser, M.; Treutler, O.; Ahlrichs, R. *Chem. Phys. Lett.* **1997**, *264*, 573. (d) Hirata, S.; Head-Gordon, M. *Chem. Phys. Lett.* **1999**, *314*, 291. (e) Casida, M. E.; Salahub, D. R. *J. Chem. Phys.* **2000**, *113*, 8918. (f) Hirata, S.; Zhan, C.-G.; Aprà, E.; Windus, T. L.; Dixon, D. A. *J. Phys. Chem. A* **2003**, *107*, 10154. (g) Zhan, C.-G.; Nicholas, J. A.; Dixon, D. A. *J. Phys. Chem. A* **2003**, *107*, 4184.
- (47) Frisch, M. J.; Trucks, G. W.; Schlegel, H. B.; Scuseria, G. E.; Robb, M. A.; Cheeseman, J. R.; Montgomery, J. A., Jr.; Vreven, T.; Kudin, K. N.; Burant, J. C.; Millam, J. M.; Iyengar, S. S.; Tomasi, J.; Barone, V.; Mennucci, B.; Cossi, M.; Scalmani, G.; Rega, N.; Petersson, G. A.; Nakatsuji, H.; Hada, M.; Ehara, M.; Toyota, K.; Fukuda, R.; Hasegawa, J.; Ishida, M.; Nakajima, T.; Honda, Y.; Kitao, O.; Nakai, H.; Klene, M.; Li, X.; Knox, J. E.; Hratchian, H. P.; Cross, J. B.; Bakken, V.; Adamo, C.; Jaramillo, J.; Gomperts, R.; Stratmann, R. E.; Yazyev, O.; Austin, A. J.; Cammi, R.; Pomelli, C.; Ochterski, J. W.; Ayala, P. Y.; Morokuma, K.; Voth, G. A.; Salvador, P.; Dannenberg, J. J.; Zakrzewski, V. G.; Dapprich, S.; Daniels, A. D.; Strain, M. C.; Farkas, O.; Malick, D. K.; Rabuck, A. D.; Raghavachari, K.; Foresman, J. B.; Ortiz, J. V.; Cui, Q.; Baboul, A. G.; Clifford, S.; Cioslowski, J.; Stefanov, B. B.; Liu, G.; Liashenko, A.; Piskorz, P.; Komaromi, I.; Martin, R. L.; Fox, D. J.; Keith, T.; Al-Laham, M. A.; Peng, C. Y.; Nanayakkara, A.; Challacombe, M.; Gill, P. M. W.; Johnson, B.; Chen, W.; Wong, M. W.; Gonzalez, C.; Pople, J. A. *Gaussian 03*, Revision E.01; Gaussian, Inc.: Wallingford, CT, 2004.
- (48) (a) Dunlap, B. I. *J. Chem. Phys.* **1983**, *78*, 3140. (b) Dunlap, B. I. *J. Mol. Struct. (THEOCHEM)* **2000**, *529*, 37.
- (49) Werner, H.-J.; Knowles, P. J.; Lindh, R.; Manby, F. R.; Schütz, M.; Celani, P.; Korona, T.; Rauhut, G.; Amos, R. D.; Bernhardsson, A.; Berning, A.; Cooper, D. L.; Deegan, M. J. O.; Dobbyn, A. J.; Eckert, F.; Hampel, C.; Hetzer, G.; Lloyd, A. W.; McNicholas, S. J.; Meyer, W.; Mura, M. E.; Nicklass, A.; Palmieri, P.; Pitzer, R.; Schumann, U.; Stoll, H.; Stone, A. J.; Tarroni, R.; Thorsteinsson, T. *MOLPRO*, version 2006.1, a package of ab initio programs; see <http://www.molpro.net>.
- (50) (a) Bylaska, E. J.; de Jong, W. A.; Kowalski, K.; Straatsma, T. P.; Valiev, M.; Wang, D.; Aprà, E.; Windus, T. L.; Hirata, S.; Hackler, M. T.; Zhao, Y.; Fan, P.-D.; Harrison, R. J.; Dupuis, M.; Smith, D. M. A.; Nieplocha, J.; Tippuraj, V.; Krishnan, M.; Auer, A. A.; Nooijen, M.; Brown, E.; Cisneros, G.; Fann, G. I.; Frücht, H.; Garza, J.; Hirao, K.; Kendall, R.; Nichols, J. A.; Tsemekhman, K.; Wolinski, K.; Anchell, J.; Bernholdt, D.; Borowski, P.; Clark, T.; Clerc, D.; Dachs, H.; Deegan, M.; Dyall, K.; Elwood, D.; Glendening, E.; Gutowski, M.; Hess, A.; Jaffe, J.; Johnson, B.; Ju, J.; Kobayashi, R.; Kutteh, R.; Lin, Z.; Littlefield, R.; Long, X.; Meng, B.; Nakajima, T.; Niu, S.; Pollack, L.; Rosing, M.; Sandrone, G.; Stave, M.; Taylor, H.; Thomas, G.; van Lenthe, J.; Wong, A.; Zhang, Z. *NWChem, A Computational Chemistry Package for Parallel Computers*, Version 5.1; Pacific Northwest National Laboratory: Richland, WA, 2007. (b) Kendall, R. A.; Aprà, E.; Bernholdt, D. E.; Bylaska, E. J.; Dupuis, M.; Fann, G. I.; Harrison, R. J.; Ju, J.; Nichols, J. A.; Nieplocha, J.; Straatsma, T. P.; Windus, T. L.; Wong, A. T. *Comput. Phys. Commun.* **2000**, *128*, 260.
- (51) Cotton, F. A.; Murillo, C. A.; Walton, R. A. *Multiple Bonds Between Metal Atoms*, 3rd ed.; Springer: New York, 2005.
- (52) Bino, A.; Cotton, F. A.; Dori, Z.; Sekutowski, J. C. *Inorg. Chem.* **1978**, *17*, 2946.
- (53) (a) Budzichowski, T. A.; Chisholm, M. H.; Folting, K.; Huffman, J. C.; Streib, W. E. *J. Am. Chem. Soc.* **1995**, *117*, 7428. (b) Lopez, L. P. H.; Schrock, R. R. *J. Am. Chem. Soc.* **2004**, *126*, 9526.
- (54) (a) Levisalles, J.; Rose-Munch, F.; Rudler, H.; Daran, J.-C.; Jeannin, Y. *J. Chem. Soc., Chem. Commun.* **1981**, 1057. (b) Abrahamson, H. B.; Heeg, M. J. *Inorg. Chem.* **1984**, *23*, 2281.
- (55) Li, S.; Hennigan, J. M.; Dixon, D. A.; Peterson, K. A. *J. Phys. Chem. A* **2009**, *113*, 7861.
- (56) Chase, M. W., Jr. *NIST-JANAF Thermochemical Tables*, 4th ed. *J. Phys. Chem. Ref. Data* **1998**, Monogr 9 (Suppl. 1).
- (57) Grimley, R. F.; Burns, R. P.; Inghram, M. G. *J. Chem. Phys.* **1961**, *34*, 664.
- (58) DeMaria, G.; Burns, R. P.; Drowart, J.; Inghram, M. G. *J. Chem. Phys.* **1960**, *32*, 1373.
- (59) Chupka, W. A.; Berkowitz, J.; Giese, C. F. *J. Chem. Phys.* **1959**, *30*, 827.
- (60) Ackermann, R. J.; Rauh, E. G. *J. Phys. Chem.* **1963**, *67*, 2596.
- (61) Feller, D.; Peterson, K. A.; Dixon, D. A. *J. Chem. Phys.* **2008**, *129*, 204105.

JP9082008